Tissue and Cell 89 (2024) 102454

Contents lists available at ScienceDirect

Tissue and Cell

journal homepage: www.elsevier.com/locate/tice

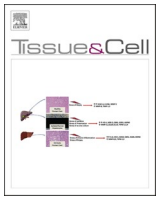

Effect of Selenium nanoparticles on Paraquat-induced-neuroinflammation and oligodendocyte modulation: Implication of the Janus kinase 2 (JAK2)/ signal transducer and activator of transcription 3 (STAT3) signaling pathway

Reda Abdelnasser Imam [a], Fatma E. Hassan [b,c], Isra H. Ali [d,e], Mansour A. Alghamdi [f,g], Basma Emad Aboulhoda [a,*,1]

[a] Department of Anatomy and Embryology, Faculty of Medicine, Cairo University, Cairo, Egypt
[b] Medical Physiology Department, Kasr Alainy, Faculty of Medicine, Cairo University, Giza 11562, Egypt
[c] General Medicine Practice Program, Department of Physiology, Batterjee Medical College, Jeddah 21442, Saudi Arabia
[d] Department of Pharmaceutics, Faculty of Pharmacy, University of Sadat City, P.O. Box 32897, Sadat City, Egypt
[e] Nanomedicine Laboratory, Faculty of Pharmacy, University of Sadat City, P.O. Box 32897, Sadat City, Egypt
[f] College of Medicine, King Khalid University, Abha 62529, Saudi Arabia
[g] Genomics and Personalized Medicine Unit, The Center for Medical and Health Research, King Khalid University, Abha 62529, Saudi Arabia

ARTICLE INFO

Keywords:
Paraquat
JAK2/STAT3
SNPC
Cerebellum
Neuro-inflammation
Selenium nanoparticles

ABSTRACT

Background: Paraquat (PQ), is an extensively used herbicide and is a well-established powerful neurotoxin. However, the mechanism underlying its neurotoxicity still needs further investigation.
Aim of work: The study investigated the pathogenesis of PQ-induced neuroinflammation of the substantia nigra pars compacta (SNPC) and cerebellum and evaluated the potential effect of selenium nanoparticles (SeN) against such neurotoxicity.
Methods: Thirty-six mice were randomly divided into three groups; Control group, PQ group: mice received PQ 10 mg/kg (i.p), and PQ + SeN group; mice received PQ in addition to oral SeN 0.1 mg/kg. All regimens were administered for 14 days. The mice's brains were processed for biochemical, molecular, histological, and immune-histochemical assessment.
Results: SeN increased the SNPC and cerebellum antioxidants (reduced glutathione, glutathione peroxidase, and superoxide dismutase 1) while decreasing malondialdehyde concentration. Also, SeN increased the anti-inflammatory interleukin (IL)-10 and decreased the pro-inflammatory IL-1β and −6 along with improving the angiogenic nitric oxide and reducing caspase-1. Further, western blots of phosphorylated Janus kinase (JAK2)/ signal transducer and activator of transcription3 (STAT3) proteins showed a significant decline. Those improving effects of SeN on SNPC, and cerebellum were supported by the significantly preserved dopaminergic and Purkinje neurons, the enhanced myelin fibers on Luxol fast blue staining, and the marked increase in Olig-2, Platelet-derived growth factor-alpha, and tyrosine hydroxylase immunoreactivity.
Conclusion: SeN could mitigate PQ-induced neurotoxicity via its antioxidant, anti-inflammatory, and anti-apoptotic properties.

1. Introduction

Exposure to environmental pollutants represents an emerging health threat. Paraquat (PQ) dichloride (1,1́-dimethyl-4–4́-bipyridylium dichloride) is a highly prevalent herbicide used in the control of weeds and grass (Fakhrabad et al. 2022). However, acute as well as long-term PQ use entails a serious health risk due to its accompanying various organs- including brain- dysfunction (Dai et al. 2020; Chen et al., 2021). PQ can cross the blood-brain barrier (BBB) via neutral amino acid transporters attaining neurotoxic levels, which in turn promotes

* Correspondence to: Department of Anatomy and Embryology Faculty of Medicine, Cairo University, Egypt
E-mail addresses: basma.emad@kasralainy.edu.eg, doctor.basma@hotmail.com (B.E. Aboulhoda).
[1] ORCID iD is 0000–0001-5582–7089.

https://doi.org/10.1016/j.tice.2024.102454
Received 18 February 2024; Received in revised form 11 May 2024; Accepted 18 June 2024
Available online 19 June 2024

neurodegenerative disorders in many regions of the brain such as substantia nigra (SN), hippocampus, and frontal cortex (Colle and Farina, 2021).

PQ neurotoxicity might be owed to the amplified generation of reactive oxygen species (ROS) and reactive nitrogen species, proinflammatory mediators such as interleukin-6 (IL-6), tumor necrosis factor-α (TNF-α), and interleukin-1β (IL-1β) besides neutrophil aggregation, and enhanced pro-inflammatory activity of astrocytes (Costa et al., 2020; Tong et al., 2022). Moreover, *Huang et al.* addressed that PQ exposure contributes to neuroinflammation via the hippocampus microglia through dysregulation of the Janus kinase (JAK2)/ signal transducer and activator of transcription3 (STAT3) signaling pathway (Huang et al., 2019). However, the neurotoxic mechanism by which exposure to PQ promotes neurodegeneration is still somewhat enigmatic. To our knowledge, the U.S. Food and Drug Administration (FDA) has not yet endorsed any medication for PQ poisoning neither prophylactic nor curative (Guo et al., 2020).

Selenium (Se) is a naturally occurring metal-like element that is essential for human health through the activities of its various selenoproteins (Cruz et al., 2023). Se maintains various biological functions within the physiological range, including redox homeostasis, growth, and immunity (Au et al., 2023). However, the toxicity of Se remains a major concern for in vivo applications therefore its dose should be considered, which confines its bioavailability (Banerjee et al., 2022). To overcome this concern, selenium nanoparticles (SeN) exhibiting high bioavailability and bioactivity have been proposed as a promising treatment line (Hu et al., 2023).

SeN have become increasingly popular in biomedical applications for oxidative stress (OS)-induced diseases like Parkinson's disease (PD) (Salaramoli et al., 2023), and neuroinflammation by modulating microglia, inhibiting neuronal apoptosis (Hu et al., 2023), improving cognitive impairment (Ashraf et al., 2023), restoring dopamine and norepinephrine secretion and alleviating depression by inhibiting the JAK2-STAT3 pathway (Yang et al., 2022)

Therefore, we postulated that SeN, with their distinctive biological activities, could exhibit neuroprotective effects against PQ-induced neurotoxicity in the context of their antioxidant, anti-inflammatory, and anti-apoptotic properties.

2. Material and methods

2.1. Material

Sodium selenite (Na_2SeO_3, 99 %), citric acid monohydrate (reagent grade, 98 %), polyvinyl alcohol (PVA, fully hydrolyzed, MW 30,000), and ethanol (absolute, 99 %) have been purchased from Sigma Aldrich, Germany. Paraquat was supplied as paraquat dichloride purchased from Sigma-Aldrich (Cat#856177).

2.2. Methods

2.2.1. Preparation of selenium nanoparticles

Selenium nanoparticles were prepared using the wet chemical method where sodium selenite and citric acid were used as selenium precursor and reducing agent (Hassan et al., 2021; Alhawiti, 2022). Briefly, sodium selenite was dissolved in 0.05 % PVA aqueous solution to prepare 40 mM of precursor solution. Afterward, the citric acid solution was added dropwise while stirring into sodium selenite solution to prepare nanosuspension of selenium nanoparticles. Citric acid was used as both reducing and stabilizing agent for the produced nanoparticles. Furthermore, PVA was used as a surfactant to prevent aggregation of the formed nanoparticles. The solution was left on a magnetic stirrer at 90 ° C for 2 hours till obtaining the nanosuspension of selenium nanoparticles. Afterward, the nanosuspension was centrifuged for 15 minutes at 12,000 rpm to obtain the produced nanoparticles. Then, the nanoparticles were washed with ethanol (3 times) followed by distilled water (3 times). Finally, the nanoparticles were dried in an oven overnight at 75 ° C.

2.2.2. Characterization of selenium nanoparticles

Selenium nanoparticles were fully characterized to investigate their morphological, chemical, and physical features.

2.2.2.1. Morphological characterization. Selenium NPs were investigated morphologically using transmission electron microscopy (TEM, Jeol, JEM-1230, Japan). A drop of diluted selenium nanosuspension in deionized water was left on a copper mesh grid coated with carbon for 10 minutes before being stained with phosphotungstic acid. Finally, the sample specimen was completely dried before being imaged (Hamdi et al., 2023).

2.2.2.2. Size and surface charge. Both the size and surface charge of the developed selenium nanoparticles were investigated using Nanosizer ZS Series (Malvern Instruments, UK). Selenium nanosuspension was diluted by 10 folds with deionized water. Afterward, both size and zeta potential were estimated as an indication of size distribution as well as stability, respectively (Ali et al., 2023).

2.2.2.3. UV-visible spectroscopy. Diluted selenium nanosuspension in deionized water was investigated using a UV–visible double-beam spectrophotometer (Evolution 201, Thermo Scientific, UK). The sample was scanned in the range of 200–400 nm, where deionized water was placed as a blank (Alhawiti, 2022).

2.2.2.4. Fourier Transform Infrared Spectroscopy (FTIR). The chemical structure of the developed selenium nanoparticles was examined using FTIR spectroscopy (Thermoscientific, USA). The sample was analyzed within the 400–4000 cm^{-1} spectrum range (Kim et al., 2017).

2.2.2.5. X-ray Diffraction (XRD). The crystallite size of the developed selenium nanoparticles was further investigated using XRD (Philips X'Pert system, The Netherlands). The sample was analyzed in the presence of Cu Kα radiation at 40 kV and 30 mA within the 2θ range of 10−60° (Mahamuni et al., 2019). Afterward, the obtained data were utilized to obtain the crystallite size of selenium nanoparticles using Sherrer's equation (Alhawiti, 2022) as shown below, where d is the crystallite size, K is a dimensionless shape factor (0.9), λ is the wavelength (0.154060 nm), β is the line broadening at half of the maximum intensity (FWHM), and θ is Bragg's diffraction angle (Mahamuni et al., 2019).

$$d = \frac{K\lambda}{\beta Cos\ \theta}$$

2.3. Study design

All the procedures were approved by the Institutional Committee for Ethical Care and Use of Laboratory Animals (CU-IACUC No: CU-III-F-65–22) and rigorously complied with the ARRIVE guidelines of animal research ethics and the revised Animals (Scientific Procedures) Act 1986 in the UK and Directive 2010/63/EU in Europe and the National Institutes of Health guide for the care and use of Laboratory animals (NIH Publications No. 8023, revised 1978). Thirty-six mice of average weight 20–30 gm, were housed in pathogen-free standard cages at a room temperature of 25 ± 2°C, fed normal animal chow, exposed to a 12:12-h daylight/darkness, and acclimatized to the research environment for two weeks before the commencement of the study. Three groups of mice were equally allocated for this work as follows: the C*ontrol group*; mice received intravenous (I.V.) saline (vehicle of PQ), the *PQ group*; received PQ in a dosage of 10 mg/kg i.p. (Smeyne et al., 2016; Wang et al., 2017; Zeng et al., 2018; El-Gamal et al., 2021) and *PQ+SeN group* in which mice received PQ in addition to SeN in a dosage of 0.1 mg/kg by oral

gavage (Bai et al., 2017; Karami et al., 2018; Elfakharany et al., 2021; Kondaparthi et al., 2021). All study regimens were administered for 2 weeks, and then the mice were euthanized via pentobarbital injection followed by cervical dislocation. During the whole experiment, no signs of SeN toxicity were observed.

The mice's brains were obtained via careful dissection. Six randomly chosen brains were used for biochemical and molecular analysis, and the other six were preserved in formalin. Paraffin blocks were prepared and employed for histological Hematoxylin & Eosin (H&E), and Luxol fast blue staining as well as immune-histochemical assessment.

2.4. Biochemical parameters

Tissue homogenates of the cerebellar and substantia nigra samples underwent ELISA testing for the OS markers: malondialdehyde (MDA), reduced glutathione (GSH), glutathione peroxidase (GPX), and superoxide dismutase 1 (SOD1) as well as the inflammatory biomarkers interleukin-1β (IL-1β), interleukin-6 (IL-6) and interleukin-10 (IL-10), besides the assay of nitric oxide (NO) as an angiogenic factor and caspase-1 as an apoptotic marker as per the manufacturer's recommendations. Biochemical kits are demonstrated in (Table 1).

2.4.1. Western blotting analysis of brain tissue JAK2/STAT3 proteins

Fifty mg of tissue samples from the substantia nigra and cerebellum were added to 1 ml of Trilfast, and homogenates underwent protein precipitation. Electrophoresed proteins on SDS-PAGE were transferred to a Hybond™ nylon membrane (GE Healthcare) via TE62 Standard Transfer Tank. Additionally, β-actin (abcam, ab8227) was applied as a housekeeping protein. The membrane was incubated overnight at 4°C in an antibody solution containing, JAK2 Antibody (C-10): sc-390539 (Santa Cruz) and anti-STAT3 antibody (Abcam, EPR787Y). The membrane was then incubated for 1 hour at room temperature in an antibody Solution containing appropriate dilution of HRP-conjugated secondary antibody. A gel documentation system (Geldoc-it, UVP, England) was applied for data analysis using Totallab analysis software (Ver.1.0.1).

2.4.2. Histological study

The brain specimens were subjected to routine fixation in a 10 % formol saline solution and paraffin processing. Sections of 4 μm thickness were stained with hematoxylin and eosin, and Luxol fast blue staining for assessment of myelination (Kiernan, 2000).

Table 1
Biochemical markers.

Marker	Company	Catalog# No	City, state, and Country
Reduced Glutathione (GSH)	Abcam	ab235670 (Fluorometric)	Waltham, Massachusetts, USA
Glutathione Peroxidase (GPX)		ab102530 (Colorimetric)	
Superoxide Dismutase 1 (SOD 1)		ab285309 (Colorimetric)	
Malondialdehyde (MDA)		ab238537 (Competitive ELISA)	
Interleukin-1 beta (IL-1 β)		ab100704 (Colorimetric)	
Interleukin-6 (IL-6)		ab222503 (Colorimetric)	
Interleukin-10 (IL-10)		ab108870 (Colorimetric)	
Nitric oxide (NO)	SunLong Biotech Co., LTD	SL0615Mo	Hangzhou City, Zhejiang Province, China
Capase-1	Elabescience	E-EL-M0201	Houston, Texas, USA

2.4.3. Immunohistochemical study

The immunohistochemical study was performed via the avidin-biotin peroxidase technique as previously described (Hassan et al., 2023). The deparaffinized sections underwent heat-mediated antigen retrieval in a microwave oven in 0.01 mol/l citrate buffer (pH 6). For quenching of the endogenous peroxidase activity, the sections were incubated in 0.3 % H_2O_2 for 30 min before blocking with 5 % horse serum for 2 h. The primary antibodies used are tyrosine hydroxylase (TH) (dilution 1:200), TNF-α (dilution 1:200), platelet-derived growth factor receptor alpha (PDGFRα) (dilution 1:200), and oligodendrocyte transcription factor-2 (Olig-2) (dilution 1:100) in an automated Dako autostainer (Dako En Vision Flix). HRP was utilized as the secondary antibody. The sections were developed with 0.05 % diaminobenzidine (DAB) slides as chromogen (Amersham, Little Chalfont, UK), counterstained with Mayer's Hematoxylin, dehydrated, cleared, and mounted with DPX. Negative controls were processed according to the same protocol, except for the use of the primary antibody in the autostainer. Positive controls were kidney tissue sections for PDGFRα, brain striatal tissue for TH, tonsillar tissue for TNF-α and oligodendroglioma tissue for Olig-2.

The Immunohistochemical kits are demonstrated in (Table 2).

2.4.4. Histomorphometric study

The histomorphometric study was done via Leica Qwin 500 C, Leica Image Analysis System Ltd. Affixed to a Leica ICS150 HD microscope camera (Cambridge, United Kingdom), in six live random fields. The histomorphometric study included:

1) Estimation of cerebellar cortical thickness (c) at the mid-sagittal section of the cerebellum in the middle of the folium facing the fissure (×100).
2) Estimation of the granular layer (g) and molecular layer (m) thickness (×100).
3) Estimation of the distance between the folia (d) (×100).
4) Estimation of the count of degenerated neurons at the SNPC and the count of apoptotic Purkinje cell count at 40× magnification (×400).
5) Evaluation of the area percentage of the immunohistochemical expression of TNF-α, PDGFRα, and Olig-2 (×400) in the immunostained sections.
6) Estimation of the count of TH immunoreactive neurons in the TH immunohistochemically stained sections (×400).
7) Morphometric evaluation the optical density of Luxol fast blue (×400).

2.5. Statistical analysis

GraphPad version 9 was adopted for statistical analysis. The results were reported as mean ± SD, with a 0.05 cut-off p-value. ANOVA was applied to compare the groups, and post-hoc Tukey's test was performed subsequently.

Table 2
Immunohistochemical markers.

Marker	Company	Catalog# No	City, state, and Country
platelet-derived growth factor receptor alpha (PDGFRα) rabbit mAb	ABclonal	A22220	Woburn, Massachusetts, USA
Tyrosine hydroxylase (TH) rabbit pAb	ABclonal Servicebio	A12756	Woburn, Massachusetts, USA
Anti-TNF-α rabbit pAb		GB11188	Wuhan, China
Anti-oligodendrocytes (Olig-2) rabbit polyclonal	GeneTex, Inc.	GTX132732	Irvine, California, USA

3. Results

3.1. Morphological characterization of SeN's

TEM image displayed in Fig. 1 illustrates the morphological features of the developed nanoparticles in terms of size and shape. It is observed that the developed nanoparticles possess spherical shapes with average size around 9 – 15 nm. This is found to be in good accordance with what has been previously reported (Alhawiti, 2022).

3.2. Size and surface charge

Both the size and surface charge of the developed selenium nanoparticles have been estimated through size and zeta potential measurement, respectively using Malvern Zeta Sizer. It was found that the developed selenium nanoparticles possess a size average of 14.63 ± 2.13 nm and a highly negative surface charge of - 23.84 ± 3.03 mV. The obtained size is found to be following the results obtained from TEM image analysis. Furthermore, the high negative surface charge of the obtained nanoparticles is expected to prevent their aggregation and indicate their high stability. This is found to be in good agreement with previous results reported in the literature (Blinov et al., 2022).

3.3. UV-visible spectroscopy

Fig. 2 demonstrates the scanning spectrum of diluted nanosuspension of selenium nanoparticles in deionized water. Maximum absorbance detected at the wavelength of 260 nm proves the successful preparation of selenium nanoparticles. Surface plasmon resonance (SPR) associated with the change in the optical properties of metallic nanoparticles including selenium nanoparticles indicates the successful formation of selenium nanoparticles. Furthermore, UV–visible spectroscopy analysis proves the stability of the formed nanoparticles over 30 days duration as below. This can be inferred from the appearance of maximum absorbance at 260 nm as shown in Fig. 2 along the 30 days study. This also matches the results obtained from the surface charges analysis that indicate the high stability of the produced nanoparticles owing to the intense negative charges. Overall, these results are found to be in good accordance with results reported in previous studies.

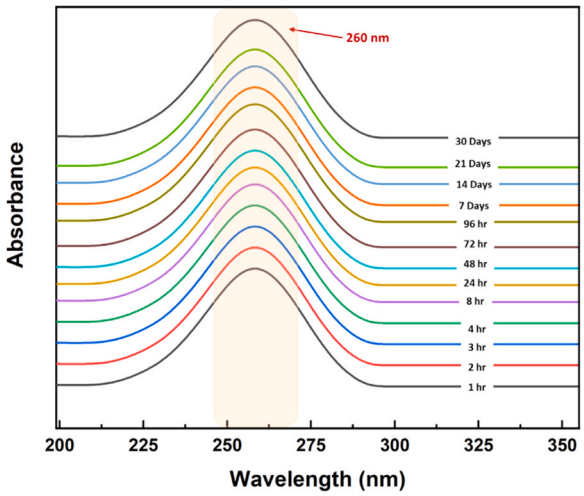

Fig. 2. UV–visible spectrum for selenium nanoparticles.

3.4. Fourier Transform Infrared Spectroscopy (FTIR)

The successful formation of selenium nanoparticles was further confirmed by investigating their chemical structure using FTIR spectroscopy as shown in Fig. 3. This was indicated by observing the characterized functional moieties for reduced selenium nanoparticles.

For instance, the broadband detected at 3546 cm^{-1} indicates the abundance of stretching of citric acid-reducing hydroxylic groups (– OH). This confirms the abundance of the hydroxylic (– OH) groups surrounding the surface of selenium nanoparticles which in turn refers to the high stability of the formed nanoparticles. In addition, the band appearing at 1625 cm^{-1} corresponds to the abundance of C═O stretching within the structure of citric acid surrounding selenium nanoparticles. Furthermore, the abundance of bands at 1145 cm^{-1} and 1412 cm^{-1} correspond to C – O and C – H bonds, respectively within the citric acid structure. Finally, the coordination bonds between selenium nanoparticles and citric acid are detected through the appearance of the band at 825 cm^{-1}. It is worth mentioning that FTIR spectrum analysis confirms the capability of citric acid to surround the formed selenium

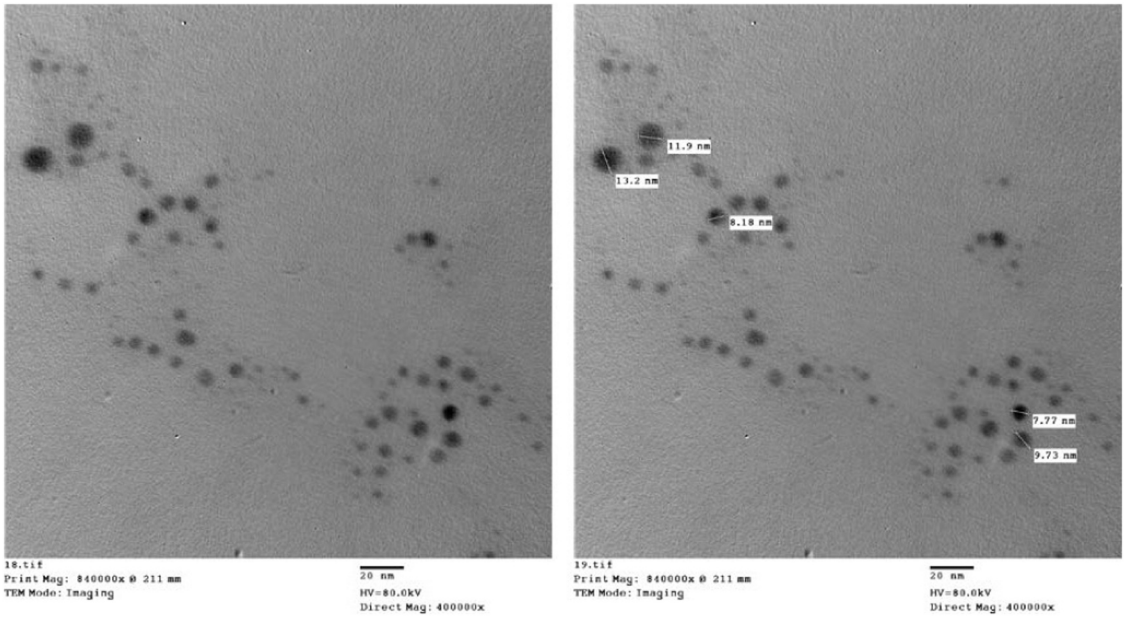

Fig. 1. Transmission electron microscopy (TEM) image displaying both the size and shape of the developed Selenium Nanoparticles (TEM x 400000, Scale Bar: 20 nm).

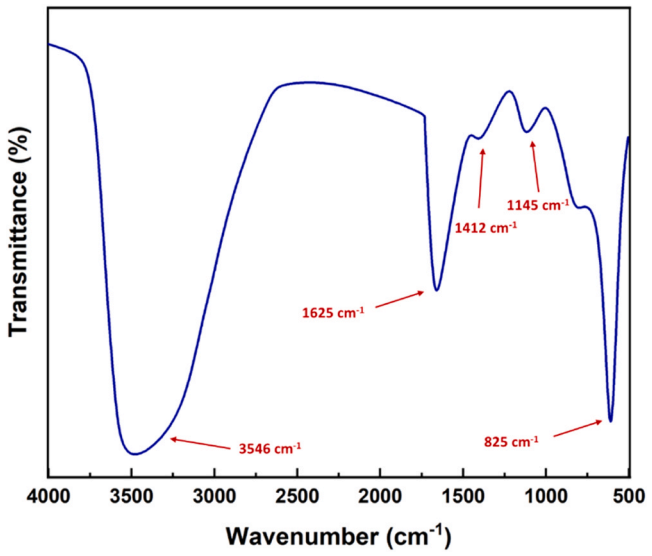

Fig. 3. FTIR spectrum for selenium nanoparticles.

nanoparticles leading to the prevention of their aggregation and thus increasing their stability. These results are found to be in good agreement with previous analyses in the literature (Hassan et al., 2021; Alhawiti, 2022; Blinov et al., 2022).

3.5. X-ray Diffraction (XRD)

Fig. 4 shows the X-ray diffractogram of the prepared selenium nanoparticles. It demonstrates characteristic sharp peaks at 2θ values of 20.6, 26.1, 32.4, 35.7, 37.9, 39.5, 44.8, 48.5, 53.2, 56.5, and 59 which confirm the successful formation of spherical-shaped selenium nanoparticles in highly crystalline form. Furthermore, the appearance of a highly intense peak at 26.1 indicates the high purity of the prepared crystalline selenium nanoparticles. Finally, according to the Scherer equation, the calculated crystallite size of the developed selenium nanoparticles was found to be 17 nm. This is found to be similar to results obtained from both TEM image analysis as well as zeta sizer measurements. Moreover, XRD diffractogram analysis was found to be in good accordance with XRD analysis reported in previous studies (El Lateef et al., 2019; Alhawiti, 2022).

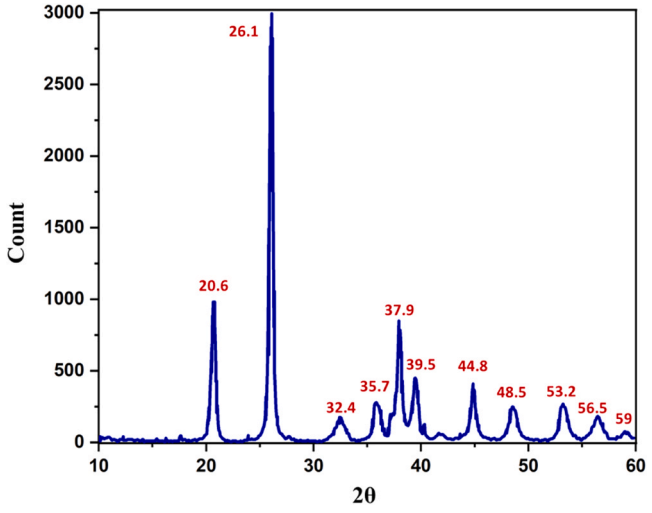

Fig. 4. XRD analysis for selenium nanoparticles.

3.6. SeN's effect on oxidative stress markers in both SNPC and cerebellum

PQ administration for 2 weeks led to significant impairment in the redox homeostasis. On the other hand, SeN administration significantly enhanced the antioxidants biomarkers GSH, GPX, and SOD in both SNPC and cerebellum. This was accompanied by significant reduction in the lipid peroxidation product MDA. Of note, the SNPC lipid peroxidation was almost totally reversed by the administration of SeN (Table 3).

3.7. SeN's effect on inflammatory/anti-inflammatory markers in the SNPC and cerebellum

Significant neuroinflammation was detected in the SNPC and cerebellar areas of the PQ group reflected by significant increase in the pro-inflammatory markers IL-1 and IL-6 along with significant decrease in the anti-inflammatory cytokine IL-10. SeN administration significantly reduced the level of IL-1 and IL-6 in the SNPC and cerebellum compared to the PQ group. In parallel, SeN enhanced IL-10 in both brain areas compared to the PQ group (Fig. 5).

3.8. SeN effect on the angiogenesis and apoptosis indicators in the SNPC and CER

In comparison to the control group, there was significant reduction in the level of the angiogenesis biomarker NO and significant elevation in the apoptotic marker caspase-1 in both SNPC and cerebella of the PQ-treated group. Treatment with SeN significantly ameliorated these alterations (Table 4).

3.9. SeN's effect on the JAK2/STAT3 protein levels in the SNPC and cerebellum

Relative to the control group, the western blotted levels of phosphorylated JAK2 and STAT3 proteins were markedly increased in the SNPC and cerebella of the PQ group. The PQ+SeN group displayed significant reduction in both JAK2 and STAT3 (Figs. 6 and 7).

3.10. Improvement of the histological architecture of the SNPC and cerebellum with SeN administration

Relative to the control group, the SNPC of the PQ group exhibited disturbed architecture, intercellular edema, and degeneration of the dopaminergic neurons. However, the PQ+ SeN group SNPC revealed preserved neurons.

The control cerebellar sections showed intact molecular, Purkinje and granular cells. The PQ group cerebella exhibited degenerated Purkinje cells, inter-Purkinje cell edema, and pale architecture of the granular layer. The PQ+SeN group exhibited preserved Purkinje cells

Table 3
Oxidative stress markers among the different groups in the SNPC and CER.

Tissue	Biomarker	Control	PQ	PQ+SeN
SNPC	GSH (ng/ml)	231.5±12.3	31.7±3.5$^{@}$	155.7±4.2$^{\#}$
	GPX (ng/ml)	196.7±6.1	50.8±6.8$^{@}$	156.9±4.8$^{\#}$
	SOD (ng /ml)	206.8±7.3	65.0±4.5$^{@}$	138.5±6.9$^{\#}$
	MDA (ng/ml)	0.7±0.1	9.3±1.0$^{@}$	1.8±0.2$^{\#}$
Cerebellum	GSH (ng/ml)	199.7±5.1	75.1±4.2$^{@}$	121.0±4.8$^{\#}$
	GPX (ng/ml)	171.7±5.5	88.9±16.6$^{@}$	119.3±4.0$^{\#}$
	SOD (ng /ml)	206.7±8.7	43.5±3.0$^{@}$	99.3±3.0$^{\#}$
	MDA (ng/ml)	0.7±0.1	4.0±0.4$^{@}$	8.1±1.0$^{\#}$

Abbreviations: PQ; Paraquat, SeN; Selenium nanoparticles, SNPC; Substantia nigra pars compacta, GSH; Reduced glutathione, GPX; Glutathione peroxidase, SOD1; Superoxide dismutase 1, MDA; Malondialdehyde. Data were represented as mean ±SD. $^{@}$: Statistically significant compared to the control group, $^{\#}$: Statistically significant compared to PQ group. *P*-value<0.05 is considered statistically significant. SD: Standard deviation.

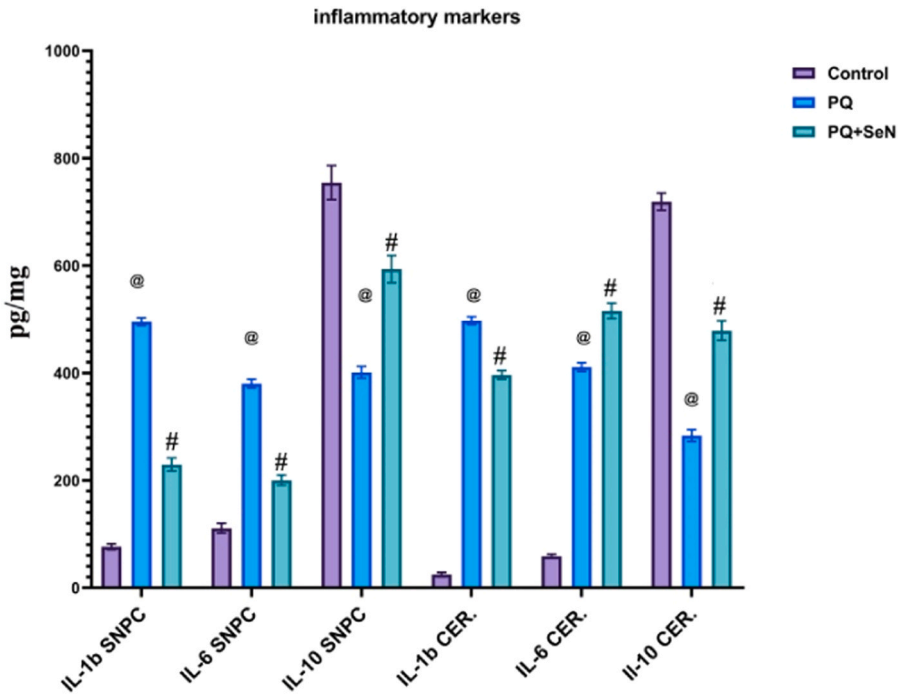

Fig. 5. Assessment of inflammatory markers Interleukin-1 beta (IL-1β), Interleukin-6 (IL-6), Interleukin-10 (IL-10) among the different study groups. Data are represented as (pg/mg), mean ± SD with $p < 0.05$ regarded as significant, (@) significant compared to control, (#) significant compared to PQ, using ANOVA, Tukey post hoc test. PQ: Paraquat, SeN: Selenium nanoparticles, SNPC; Substantia nigra pars compacta, CER; Cerebellum.

Table 4
Nitric oxide and caspase-1 levels in the SNPC and cerebellum among the different groups.

Tissue	Biomarker	Control	PQ	PQ+SeN
SNPC	NO (μmol/L)	84.0 ±3.8	43.0±2.8$^{@}$	55.5±2.8$^{\#}$
	Caspase-1 (pg/ml)	201.8±10.3	567.4±15.0$^{@}$	279.3±13.6$^{\#}$
Cerebellum	NO (μmol/L)	89.4±3.6	46.1±1.8$^{@}$	63.1±3.1$^{\#}$
	Caspase-1 (pg/ml)	0.5±0.1	5.2±0.4$^{@}$	2.0±0.2$^{\#}$

Abbreviations: PQ; Paraquat, SeN; Selenium nanoparticles, SNPC; Substantia nigra pars compacta, NO; Nitric oxide. Data were represented as mean ±SD. $^{@}$: Significant compared to control, $^{\#}$: Significant compared to PQ. *P*-value<0.05 is considered statistically significant. SD: Standard deviation.

and intact architecture of the granular layer.

3.11. Histomorphometry of the cerebellar cortical layers and the distance between the cerebellar folia

There was significant decrease in the total cortical thickness and the thickness of the molecular and granular cell layers in the PQ group compared with the control group. This was accompanied by significant increase in the distance between the cerebellar folia denoting shrinkage degeneration of the cerebellar folia. The thickness of the cerebellar cortical layers was restored with statistically significant difference in the molecular layer thickness. The distance between the folia was also significantly improved in the PQ+SeN group ($p < 0.05$) (Fig. 8).

3.12. Role of SeN on neuronal remyelination in SNPC and cerebellum detected by Luxol fast blue staining

Luxol fast blue displayed standard myelin fibers staining in the control group. The PQ group SNPC and cerebella exhibited pale staining of most of the myelin fibers. On the contrary, both neural tissues of the PQ+SeN group showed enhanced myelin staining. The histomorphometric results were supportive to the Luxol fast blue staining pattern in all groups (Fig. 9).

3.13. Effect of SeN on the PQ-induced neuroinflammation tracked by TNF-α immune-staining

TNF-α immune-stained sections of the control group showed minimal TNF-α expression. The PQ group neural tissues exhibited remarkable increase in TNF-α immuno-staining. The SNPC and cerebella of the PQ+SeN group revealed mild TNF-α immunohistochemical expression. The histomorphometric analysis of the area percentage of the positive TNFα-immunostained cells of both the SNPC and cerebellum mirrored these findings (Fig. 10).

3.14. Neuro-restorative effect of SeN on the neurotropic growth factor PDGFR-α immunohistochemical expression in the SNPC and cerebellum

Measurement of the area percentage of the oligodendrocyte precursor marker PDGFR-α immune-staining in the PQ group revealed significant decline compared to the control group. Significant increase in the PDGFR-α immunoreactivity was recorded in both the SNPC and cerebella of the PQ+SeN group relative to the PQ group ($p<0.05$) (Fig. 11).

3.15. SeN effect on the PQ-induced reduction in Olig-2 expression of oligodendrocyte cells in the SNPC and cerebellum

Olig-2, an oligodendroglia-specific marker, acts a transcription factor for stimulating the expression of myelin-associated genes in oligodendrocyte-lineage cells. Olig-2 immune-stained section of the control group in the current study showed typical Olig-2 +ve oligodendrocytes in the SNPC and CER. The PQ group SNPC revealed marked reduction in the +ve Olig-2 cells, whereas the PQ+SeN group exhibited marked increase in the olig-2 expression. The histo-morphometric measurement of the area % +ve Olig-2 staining in the SNPC and cerebellum revealed significant decline in the PQ group compared to the control, whereas it was significantly increased in the PQ+SeN group compared to the PQ group (Fig. 12).

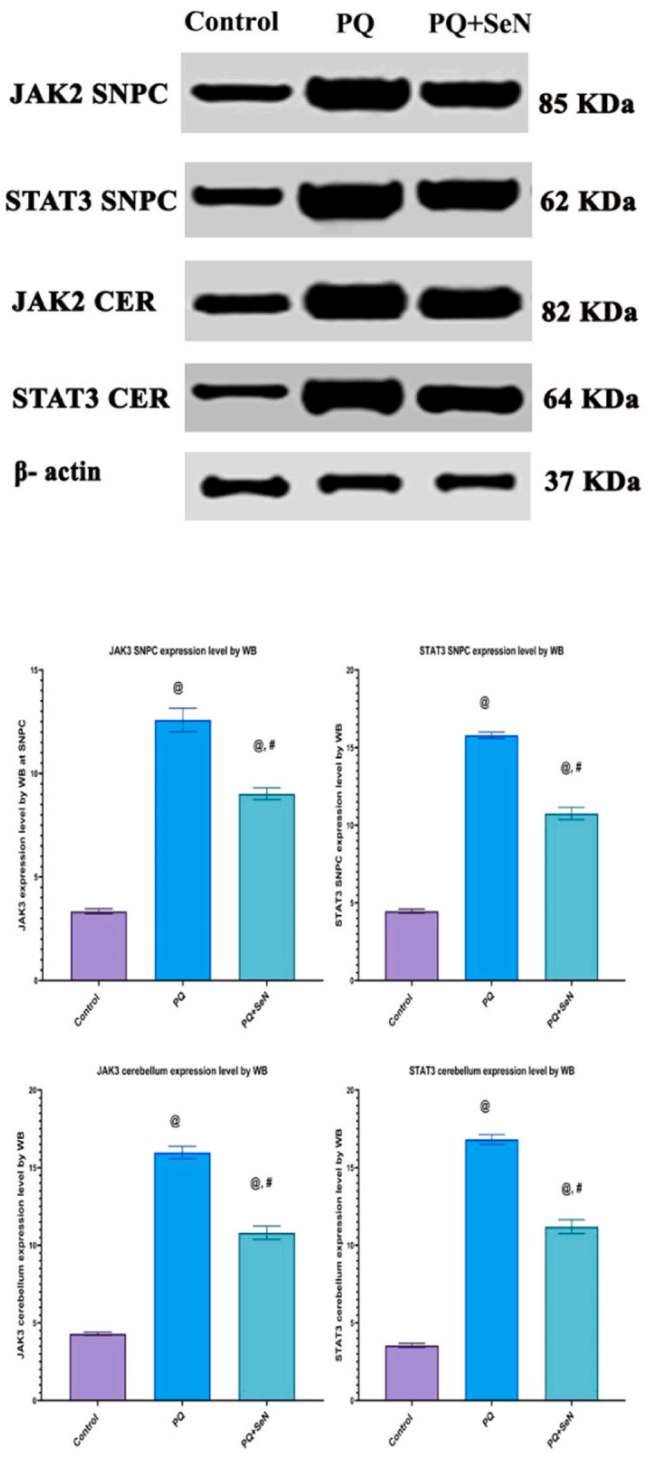

Fig. 6. Western blot for JAK3 and STAT3 in SNPC and cerebellum. JAK3 and STAT3 displayed a marked increase in the PQ group with amelioration in the PQ+SeN group. The bar charts exhibit a significant decline in the PQ+SeN compared to the PQ group regarding JAK 3 and STAT3 in the SNPC and CER. SNPC; Substantia nigra pars compacta, CER; Cerebellum. Data are expressed as mean ± SD with $p < 0.05$ regarded as significant, (@) significant compared to control, (#) significant compared to PQ, using ANOVA, Tukey post hoc test. PQ: Paraquat, SeN: Selenium nanoparticles, SNPC: substantia nigra pars compacta, CER: cerebellum.

3.16. SeN effect on the PQ-induced dopaminergic neuron degeneration in SNPC tracked by TH immune-staining

TH immune-stained sections from the control group SNPC showed standard TH-stained dopaminergic neurons. The PQ group SNPC exhibited marked neuronal loss and reduced TH immuno-staining of the remaining neurons. The SNPC of the PQ+SeN group appeared with partially preserved dopaminergic neurons. Similarly, the histomorphometric measurement of the count of TH immune-positive staining in the PQ + SeN group revealed significant increase in the PQ group compared to the control one (Fig. 13).

4. Discussion

Human health is seriously threatened by the extensive application of PQ in agricultural practices particularly in developing countries (Kannaujiya et al., 2023). By traversing the BBB, PQ potentially and preferentially disrupts microglial cells (Silva et al., 2023).

Our findings demonstrated that both SNPC and cerebellar brain tissues exhibited substantial neuroinflammation, disruption of redox homeostasis, angiogenesis, myelination, and oligodendrocyte density concurrent with significant apoptotic changes following exposure to PQ for 14 days. This is concordant with the previous studies illustrating the PQ-induced neuronal degeneration (Tong et al., 2022; Trempe and Gehring, 2023).

The PQ-induced toxicity could be related to the cycle of reduction/oxidation changes that occur to its structure (Firouzian et al., 2019). PQ is first reduced by NADPH-cytochrome c reductase to a labile radical. PQ is then oxidized by the cytochrome P-450 to a cation form, generating reactive nitrogen species (e.g. peroxynitrite anions (ONOO–)) (Sivagurunathan et al., 2023) and reactive oxygen species (e.g. superoxide anion, and hydroxyl free radicals) (Liu et al., 2011; Kheiripour et al., 2021; Miller et al., 2023). Furthermore, the liver's metabolic involvement in the detoxification of PQ (as a xenobiotic) results in the formation of ROS (Hosseini et al., 2021; Gohari-Piran et al. 2022). This cascade compromises the BBB permeability and causes selective toxic effects on the dopaminergic neurons by its monoelectronic redox cycling in the brain capillaries (Somayajulu-Niţu et al., 2009). PQ and NO also synergistically react to open the cyclosporin A-sensitive, Ca2+-dependent permeability transition pore (Fukushima et al., 2002). PQ also compromises the brain mitochondria by interfering with the conversion of nicotinamide adenine dinucleotide phosphate (NADPH) to NAD(P)+ (Naspolini et al., 2021) and by interacting with inducible nitric oxide synthase (iNOS) and NADPH oxidase type 2 (NOX2) in microglia (Hou et al., 2017; Fang et al., 2021; Tahavvori et al., 2023).

Brain lipids are crucial for the brain's structural integrity and signaling pathways (Kao et al. 2020). The brain with its high quantities of unsaturated fatty acids, low levels of antioxidant enzymes, and excessive oxygen consumption, is especially vulnerable to lipid peroxidation (Abdraboh et al., 2020; Guo et al., 2020) leading to an increase in the pro-inflammatory lipids and subsequent neurodegeneration (David and Lopez-Vales 2021; Yang et al., 2022).

Impaired brain antioxidant capacity was documented following PQ exposure through reduction of GSH outflow from glial cells (See et al., 2022) and downregulation of the antioxidant responsive element (ARE) signaling pathway and its downstream antioxidants such as GSH and SOD (Brandes and Gray, 2020; Habib et al., 2022).

Prior studies have also reported that PQ significantly increased the inflammatory cytokines TNF α, IL-1β, and IL-6, and decreased the serum levels of IL-10 (Amin et al. 2021; Nouri et al., 2021). Also, ROS are involved in the activation of inflammatory regulators such as NF-κB and COX II in the brain (Wang et al., 2021) endorsing the PQ-derived neuroinflammation in our study.

Numerous physiological functions, such as the immune system, inflammation, apoptosis, and tissue repair are regulated by the JAK/STAT signaling cascade (Hu et al., 2021). Consequently,

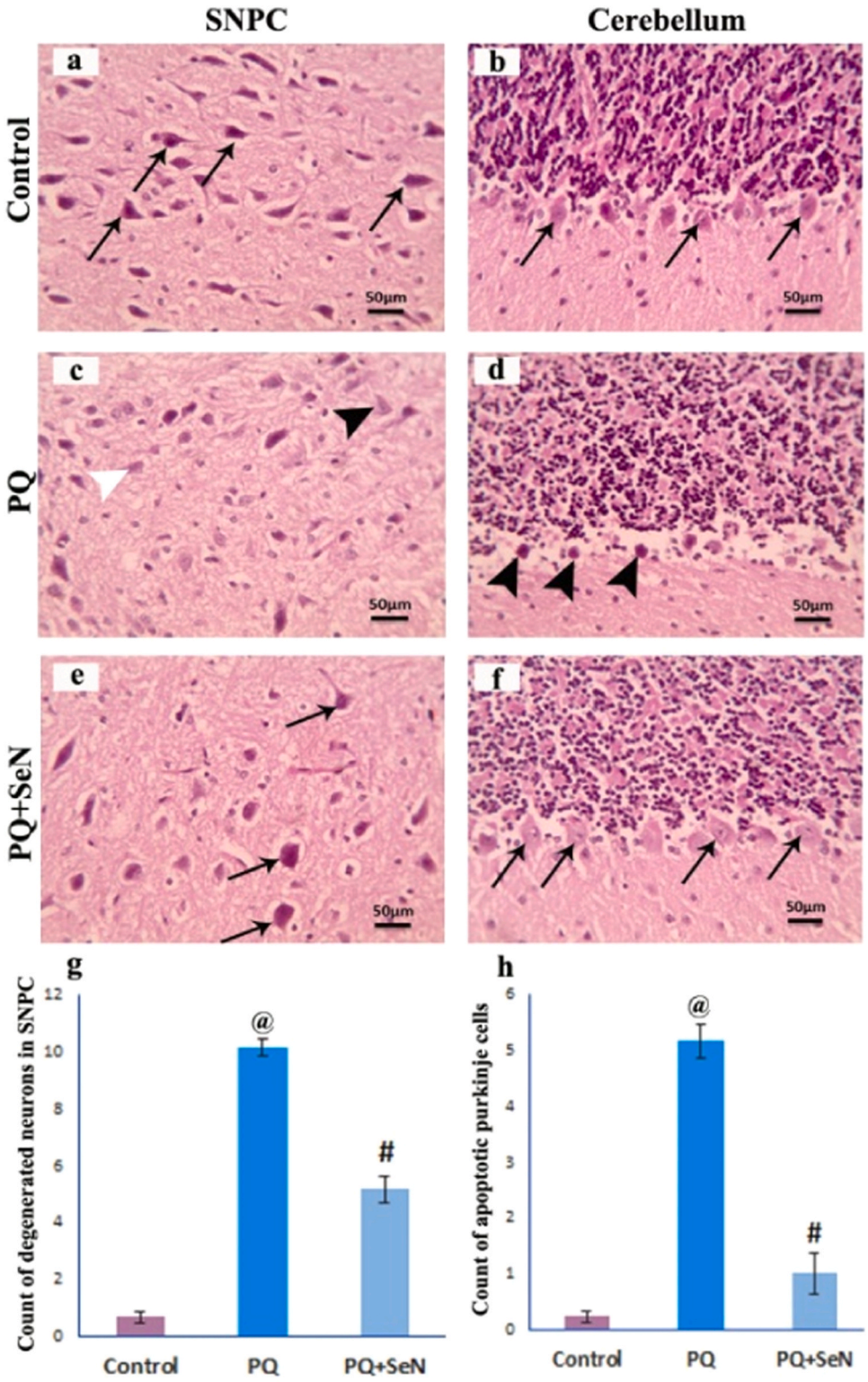

Fig. (7). Representative H&E figures of the histopathological changes in the SNPC and cerebellum. (a,b): control group (a) SNPC with normal dopaminergic neurons (arrows). (b) Cerebellum showing healthy Purkinje neurons with open face nuclei and prominent nucleoli (arrows) (c,d): PQ group (c) SNPC with pale architecture (intercellular oedema and loss of dopaminergic neurons, the remaining ones appear degenerated (white arrow head) and disfigured (black arrow head). (d): Cerebellar cortex showing red degeneration of the Purkinje neurons (black arrow heads) which appear pyknotic with marked peri-neuronal vacuolation. (e,f): PQ + SeN group (e) SNPC with numerous preserved neurons. (f): cerebellum with intact Purkinji cells (arrows) with preform soma and minimal peri-neuronal vacuolation. (Scale bar = 50 µm). (g) Count of degenerated neurons in SNPC. (h) Count of apoptotic Purkinje cells. Data are expressed as mean ± SD with $p < 0.05$ regarded as significant, (@) significant compared to control, (#) significant compared to PQ, using ANOVA, Tukey post hoc test. PQ: Paraquat, SeN: Selenium nanoparticles, SNPC: substantia nigra pars compacta.

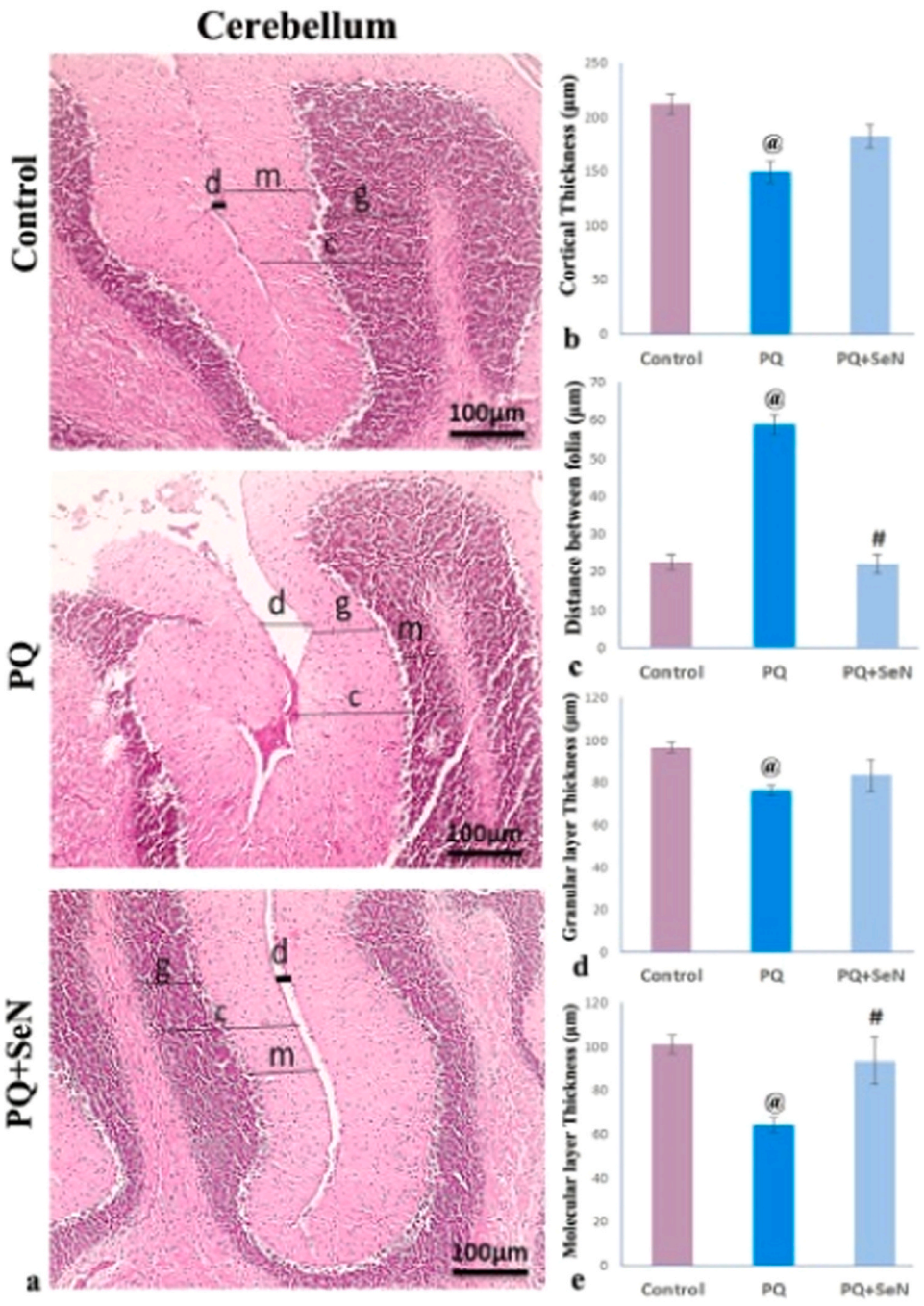

Fig. (8). Histomorphometric changes in the cerebellar cortex (a) Representative H&E figures of the morphometric measurement of the thickness of granular cell layer (g), molecular cell layer (m) and cortical layer (C) at the fundus of folia and the distance between cerebellar folia (d), (b): Cortical thickness (µm), (c): Distance between folia (µm). (d): Granular layer thickness (µm). (e): Molecular layer thickness (µm). (Scale bar = 100 µm). Data are expressed as mean ± SD with $p < 0.05$ regarded as significant, (@) significant compared to control, (#) significant compared to PQ, using ANOVA, Tukey post hoc test. PQ: Paraquat, SeN: Selenium nanoparticles, SNPC: substantia nigra pars compacta.

neurodegenerative illnesses can be attributed to dysregulations of JAK/STAT proteins (Rusek et al., 2023). It is widely recognized that OS and inflammatory cytokines particularly IL-6 cause phosphorylation of JAK2 and JAK3 in brain microglia with subsequent STAT3 activation (Li et al., 2016).

Guzzo et al. showed that JAK2/STAT3 is involved in controlling NF-κB transcription activity, as evidenced by a decrease in the p50 and p65 subunits of NF-κB's ability to bind DNA when JAK2/STAT3 is blocked (Guzzo et al., 2010; Deng et al., 2017). Therefore, activated STAT3 can trigger the synthesis and secretion of proinflammatory mediators and induce OS injury by hydrogen peroxide, thus impeding brain recovery and creating autoloop of brain damage (Chen et al., 2017a; Wang et al., 2017; Su et al., 2020). Recent studies reported hippocampus inflammatory damage by activating the JAK2/STAT3 pathway inducing M1-type polarization of microglia, and generation of pro-inflammatory cytokines such as IL-1β, iNOS, TNF-α, and IL-6 following acute PQ exposure (Zhang et al., 2021; Fan et al., 2022).

Also, dysregulated JAK2/STAT3 enhances the expression of NOD, LRR, and pyrin domain-containing protein 3 (NLRP3), mTOR, and TLRs, which cause microglial activation and contribute to neurodegeneration by way of dopaminergic neuron autophagy (Nicolas et al., 2013; Lashgari et al., 2021; Zhong et al., 2021).

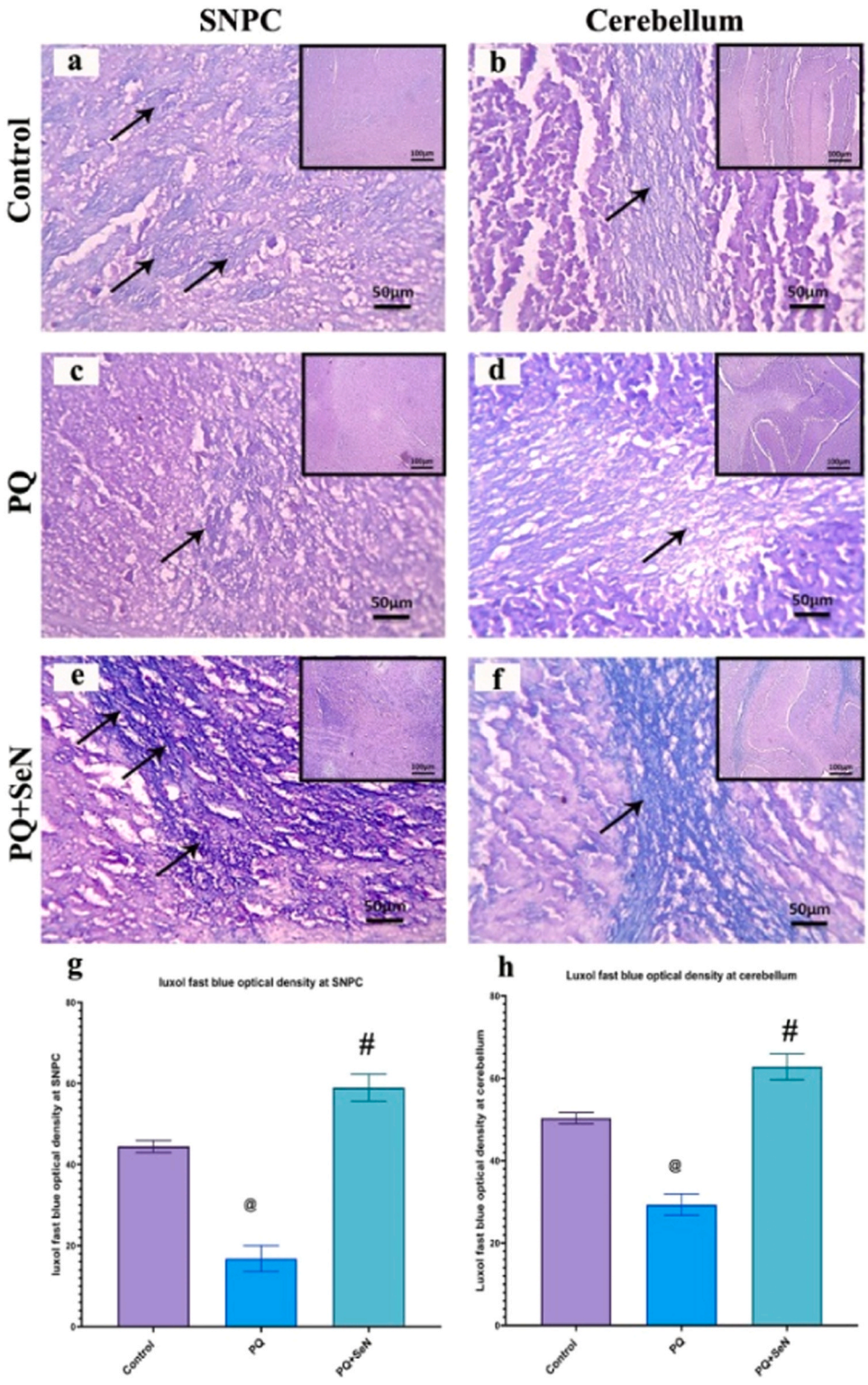

Fig. (9). Luxol fast blue representative images showing (a,b): control group with standard myelin fibers staining (black arrows). (c,d): PQ group with pale staining of most myelin fibers (white arrows). (e,f): PQ + SeN group SNPC with increased staining of myelin fibers (arrowheads). (g,h): Optical density of Luxol fast blue staining of SNPC SNPC and cerebellum, **@:** significant compared to control, #: significant compared to PQ group. (Scale bar = 100 µm). Data are expressed as mean ± SD with $p < 0.05$ regarded as significant, (@) significant compared to control, (#) significant compared to PQ, using ANOVA, Tukey post hoc test. PQ: Paraquat, SeN: Selenium nanoparticles, SNPC: substantia nigra pars compacta.

Many studies complement our results, showing that PQ exposure causes variable degrees of degeneration of dopaminergic neurons depending on the tissue vulnerability to PQ. Nonetheless, PQ's selectivity for TH-positive neurons remained constant throughout all investigations (McCormack and Di Monte, 2003; Ossowska et al., 2005; Hou et al., 2017).

Caspase-1 is the core component of all inflammasome complexes that regulate the activation, production, and secretion of IL-1β (Rand and

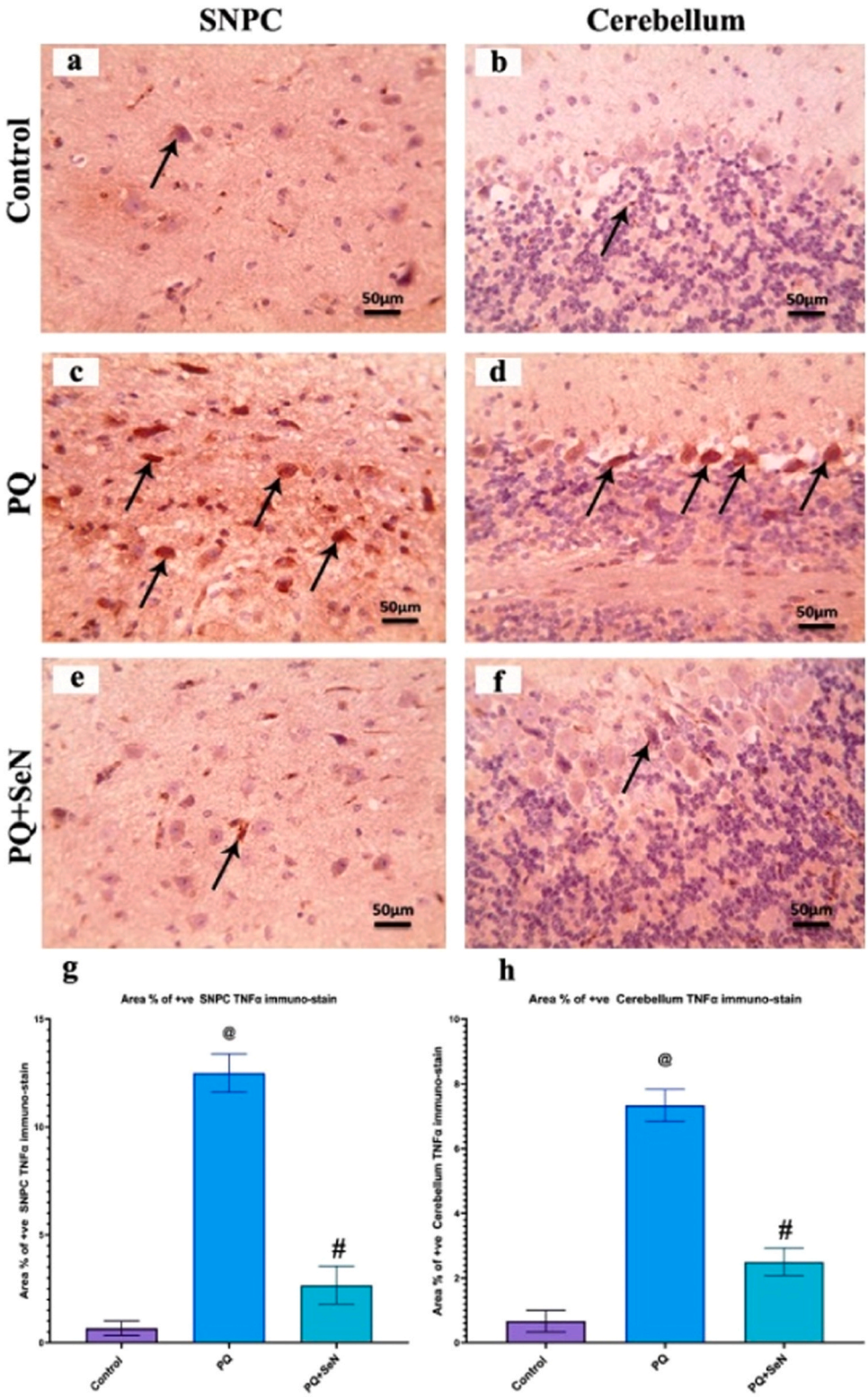

Fig. (10). TNF-α immune-stained representative images showing (a,b) control group with minimal TNF-α stained neurons (arrow). (c,d) PQ group with remarkably increased TNF-α immune-staining of the neurons (arrows). (e,f) PQ + SeN group SNPC with faintly-stained neurons. (g,h) Area percentage of TNF-α immune-reactivity of SNPC and cerebellum. (Scale bar = 50 µm). Data are expressed as mean ± SD with $p < 0.05$ regarded as significant, (@) significant compared to control, (#) significant compared to PQ, using ANOVA, Tukey post hoc test. PQ: Paraquat, SeN: Selenium nanoparticles, SNPC: substantia nigra pars compacta.

Cooper, 2021). Exposure to PQ provoked brain inflammation by hindering BBB integrity, demonstrated by increased levels of activated caspase-1 and mature IL-1β and IL-18 causing a pro-inflammatory form of programmed focal cell death in the hippocampus (Chen et al., 2015; Dai et al., 2020). However, non-canonical caspase-1 signaling cascades, independent from NLRP3, including TNF-α-mediated inflammation, have also been reported (Reinke et al., 2020).

Furthermore, excessive OS enhances the outer mitochondrial

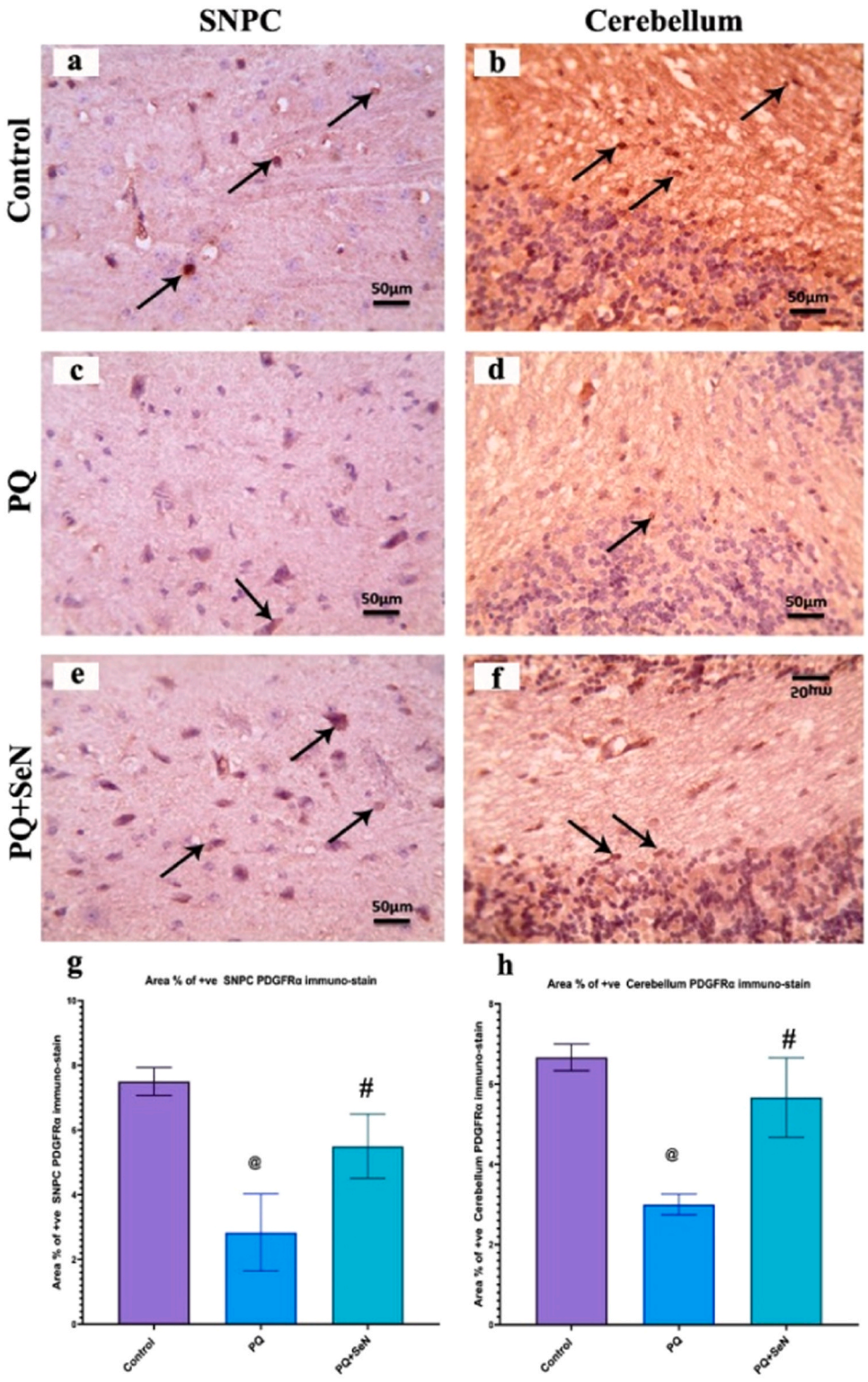

Fig. (11). PDGFR-α immune-reactivity representative images showing (a,b): control group with typical PDGFR-α staining (c,d) PQ group with few immune-stained cells (black arrow). (e,f): PQ+SeN group with restored PDGFR-α immunohistochemical expression. (d): PDGFR-α immunostaining of SNPC and cerebellum of the different study groups (Scale bar = 50 µm). Data are expressed as mean ± SD with $p < 0.05$ regarded as significant, (@) significant compared to control, (#) significant compared to PQ, using ANOVA, Tukey post hoc test. PQ: Paraquat, SeN: Selenium nanoparticles, SNPC: substantia nigra pars compacta, PDGFR-α: Platelet derived growth factor-alpha.

membrane permeability promoting the release of apoptogenic proteins known as "mitochondrial outer membrane permeabilization (MOMP)" (El-Osta and Circu, 2016). The equilibrium between pro-apoptotic (Bak and Bax) and anti-apoptotic Bcl-2 family proteins (Bcl-2) regulates this process (See et al., 2022). PQ exposure lowered Bcl-2 gene expression and increased Bax in neuroblastoma cell lines. Moreover, a Bak-dependent neuronal cell death including dose-dependent cytochrome c release, with subsequent caspase-3 activation and PARP-1

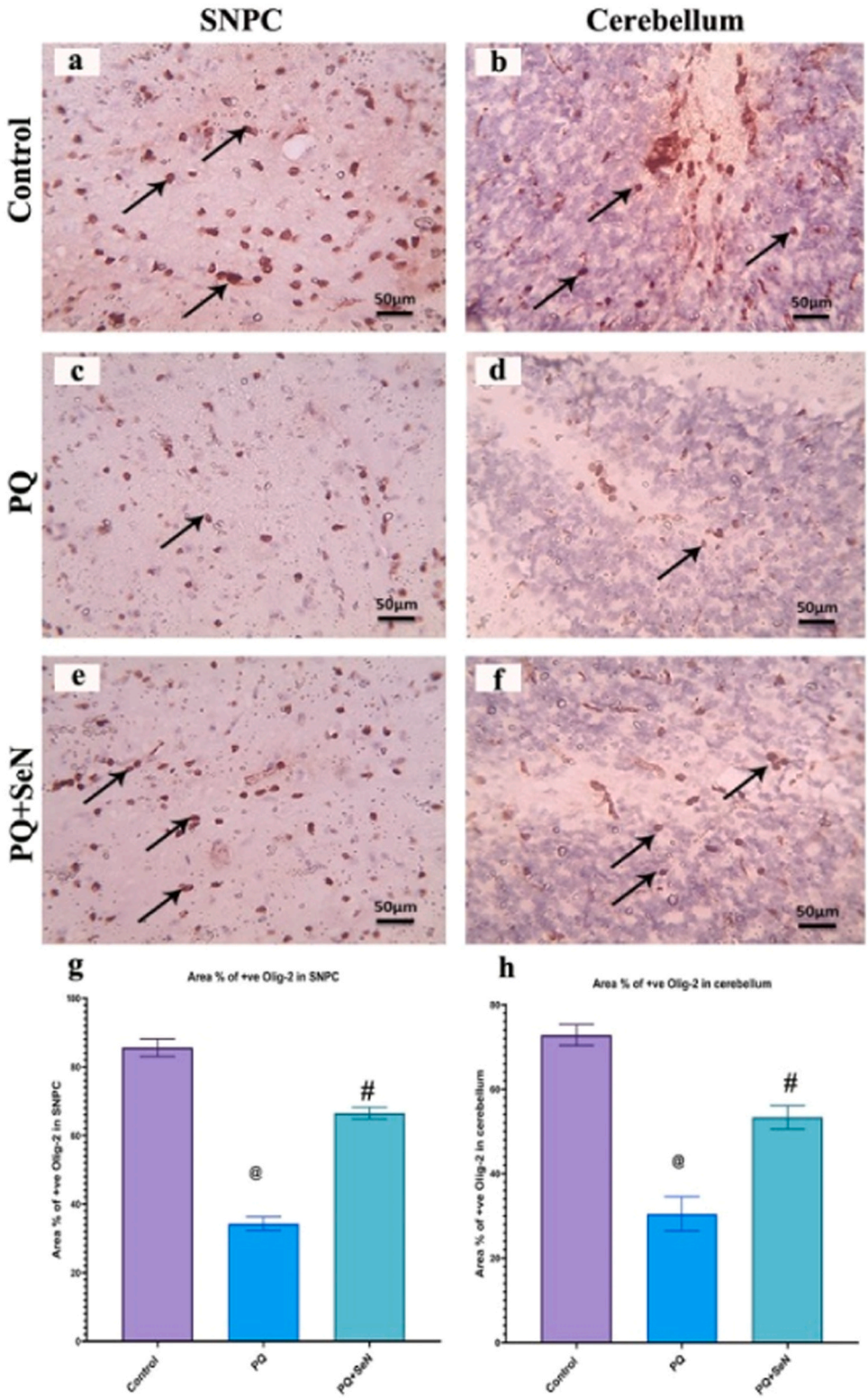

Fig. (12). Olig-2 immune-stained representative images showing (a,b): control group SNPC with typically -stained oligodendrocytes (black arrow). (c,d): PQ group SNPC with decreased stained cells. (e,f): PQ + SeN group SNPC with increased oligodendrocytes cells. (g,h): bar chart of Olig-2 staining of SNPC, (Scale bar = 50 µm). Data are expressed as mean ± SD with $p < 0.05$ regarded as significant, (@) significant compared to control, (#) significant compared to PQ, using ANOVA, Tukey post hoc test. PQ: Paraquat, SeN: Selenium nanoparticles, SNPC: substantia nigra pars compacta, Olig-2: Oligodendrocyte transcription factor 2.

cleavage was reported as a mechanism for PQ-induced neurotoxicity (Fei et al., 2008).

Nuclear protein poly (ADP-ribose) polymerase, PARP, is a highly stable protein that is essential for DNA repair (Kamaletdinova et al., 2019; Kumar et al., 2020). Neurodegenerative illnesses have been correlated with the cleavage of PARP-1 by caspase-3 (See et al., 2022). *Chinta et al.* reported a rise in the cleaved PARP protein expression following PQ intake (Chinta et al., 2008) and *Srivastav et al.* reported a

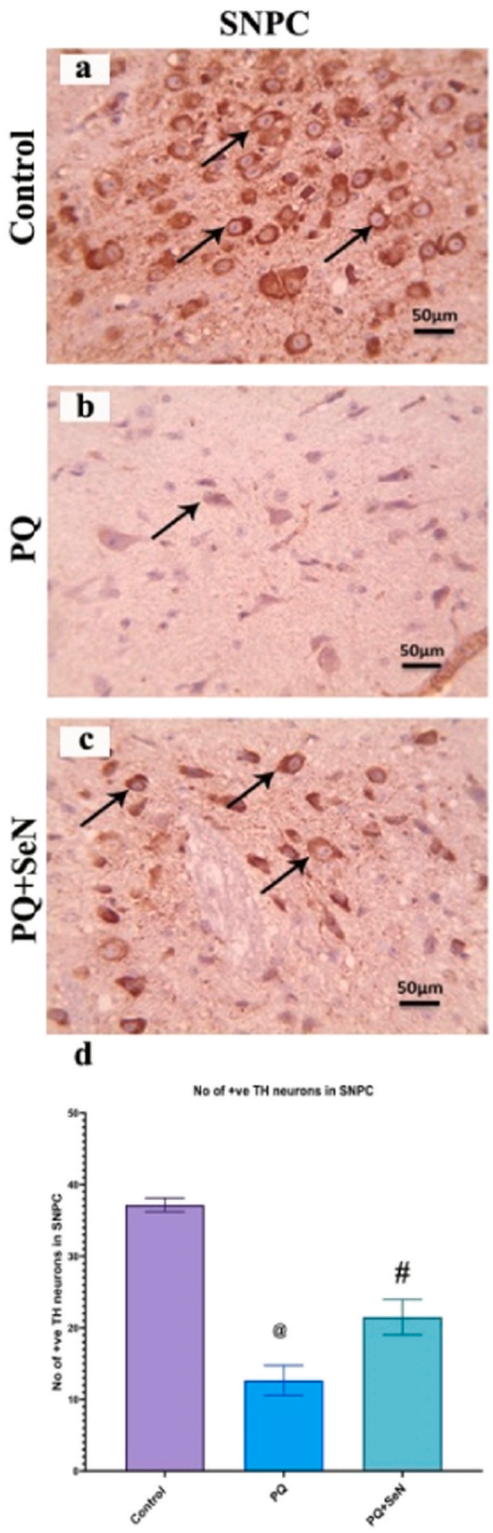

Fig. (13). TH immune-stained representative images showing (a): control group with standard TH-stained dopaminergic neurons (arrows). (b): PQ group with marked neuronal loss and reduced TH immuno-staining of the remaining neurons (arrows). (c): PQ + SeN group with partially preserved dopaminergic neurons (arrows). (d): Count of TH immunoreactive neurons in the SNPC. (Scale bar = 50 µm). Data are expressed as mean ± SD with $p < 0.05$ regarded as significant, (@) significant compared to control, (#) significant compared to PQ, using ANOVA, Tukey post hoc test. PQ: Paraquat, SeN: Selenium nanoparticles, SNPC: substantia nigra pars compacta.

significant increase in the caspase-3 expression after treatment with PQ (Srivastav et al., 2018).

Platelet-derived Growth Factor-α (PDGF-α) encourages the migration of Oligodendrocyte progenitor cells (OPCs) towards the white matter, where they differentiate into myelin-forming oligodendrocytes (Patro et al., 2022). Fyn, a non-receptor tyrosine kinase, has been shown to play a very important role in the morphological differentiation of oligodendrocytes. PQ triggers the production of ROS, thereby activating the Fyn and its downstream target c-Cbl which possess ubiquitin ligase activity resulting in the downregulation of many growth factor receptors including PDGFR-α (Cui, 2008). Also, PQ via activation of kainate receptors sensitizes oligodendrocytes to complement attack (Alberdi et al., 2006). In support of our results, apoptotic neurons were also detected by electron microscope in SN and striatum after PQ administration (Wu et al., 2013).

The critical role of OS in endothelial dysfunction has long been known. Overproduction of ROS such as superoxide causes a breakdown of NO in the vasculature. Superoxide reacts with NO, which produces peroxynitrite and causes reduced NO bioavailability therefore impaired vasorelaxation (Oztürk et al., 2015). However, the putative role of PQ in endothelial nitric oxide synthase (eNOS) expression needs further evaluation as the studies' findings are controversial. Some studies reported that exposure to PQ does not modulate the expression of eNOS (Hara et al., 2001; Ortiz-Ortiz et al., 2009), others reported that PQ via an increase of O•− 2 and other ROS has been shown to upregulate eNOS in human coronary artery endothelial cells (Zhen et al., 2008), bovine aortic endothelial cells (Drummond et al., 2000) and prostate tumor spheroids (Wartenberg et al., 2003).

Neurotoxicity treatment is challenging due to limited drug delivery, necessitating efficient substitute treatments. Nanoscale functional reconstructive materials and technologies could be a promising therapeutic paradigm for neurodegenerative diseases.

OS is one of the primary causes of neurodegenerative illnesses (Abdraboh et al., 2020; Guo et al., 2020). Consequently, various naturally occurring antioxidants were used in therapies, but their precision was limited (Ashraf et al., 2023), leading to the focus on creating nanoparticles with higher antioxidant potential.

Selenium (Se), an essential microelement, is vital for brain function and plays a crucial role in the synthesis of antioxidant enzymes like oxidoreductase and GPX (Ren et al., 2018; Shen et al., 2022). Nonetheless, SeN show superior antioxidant properties and bioavailability compared to Se compounds (Hu et al., 2023), making them effective against neurological illnesses due to their ability to penetrate the BBB (Albrakati et al., 2021; Khalil et al., 2022; Al-Omairi et al., 2022).

Our results showed that SeN intake significantly mitigated OS, neuroinflammation, and apoptosis, as well, as promoted angiogenesis, and preserved dopaminergic neurons in SNPC and cerebellum which was proven by histopathological and immunohistochemical examinations.

In accordance with our results, recent studies reported that glycine- and resveratrol-loaded SeN mitigated the neural OS (lowering the MDA level and raising GSH-PX, SOD, and total antioxidant capacity (TAC)), neuroinflammation, and neurobehavioral and motor disturbances in neurodegenerative disorders (Yue et al., 2021; Abozaid et al., 2022; Salaramoli et al., 2023). Also, *Mohamed et al.* outlined the role of the Nrf2/ARE/HO-1 defense mechanism in the neuroprotection of Rut-SeN in the hippocampus (Mohamed et al., 2023).

In many models of neurodegenerative illnesses, the SeN' anti-inflammatory activities were documented through either suppression of NF-kβ or nitric oxide synthase 2 (NOS2), and cyclooxygenase II (COX II), and their downstream molecules such as TNF-α, IL-1β, IL-6, and myeloperoxidase (MPO) (Nkpaa et al., 2019; Thabet and Moustafa, 2018; Abdelfattah et al. 2020; Albrakati et al., 2021).

Aberrant activation of the JAK2/ STAT3 pathway in response to cytokines promotes the generation of inflammatory helper T cells and various inflammation-associated genes, the activation of macrophages

and microglia resulting in acute inflammation and neuronal damage (Satriotomo et al., 2006; Camacho-Moll et al., 2021).

Through modifying JAK2/STAT3 signaling, SeN were proven to support neuronal longevity in the hippocampus (Amani et al., 2019) and lessen the effects of fluoride-induced depression which in turn inhibits microglial-mediated neuroinflammation, and IL-1β production (Yang et al., 2022). Moreover, Rutin-SeN showed an intriguing reno-protective impact by downregulating the JAK2/STAT3 and upregulating the Nrf-2/HO-1 pathways (Zaghloul et al., 2022).

Neuronal apoptosis is intimately correlated with OS and neuroinflammation (Rashid et al., 2021). Notably, the anti-apoptotic characteristics of nanoscale Se have been shown in various experimental setups (Sadek et al., 2017; Abdelfattah et al., 2020; Yuan et al., 2020; Al-Brakati et al., 2021).

SeN ameliorated the neuroinflammation by damping the gut Microbiota-NLRP3 inflammasome-caspase −1 brain axis (Yang et al., 2022). Blocking caspase-1 activation in an injured BBB can restore paracellular adhesion by averting the downregulation of Ve-cadherin, protect transport-related proteins such as caveolin-1 and LDL-R in brain vasculature, and prevent inflammatory conditions by attenuating adhesion molecules and chemokines such as ICAM-1, PECAM-1 and MCP-1 in the cellular BBB (Israelov et al., 2020). In addition, SeN can regulate p38 MAPK/ERK, NF-κB, ASK1/JNK, PI3-K/Akt/mTOR, and other signaling pathways to inhibit apoptosis induced by OS (Deng et al., 2023).

Moreover, Rutin-SeN limited the apoptotic brain damage by increasing the Bcl-2 and decreasing the caspase-3 and Bax levels in hippocampal neurons (Mohamed et al., 2023) and by their ROS scavenging activity and conservation of mitochondrial membrane integrity and permeabilization with subsequent control of cytochrome c release (Ma et al., 2018; Li et al., 2022).

NADPH oxidase (NOX) generates ROS and a proapoptotic signal through mitogen-activated protein kinase (MAPK) (Cosentino-Gomes et al. 2012). NOX overactivity was reported in PQ-induced neurotoxicity (Hou et al., 2017; Fang et al., 2021; Tahavvori et al., 2023). *Oztürk et al.* found that Se increased plasma NO levels and restored the impaired endothelium-dependent relaxation in the aorta via increasing eNOS, reducing NADPH oxidase4 (NOX4) mRNA expression owing to its antioxidant properties (Oztürk et al., 2015).

Comparing the effect of nano selenium with selenium in conventional form represents an interesting area for future research to provide better insights into the nano formulation's efficacy."

5. Conclusion

The formulated SeN significantly reduced PQ-induced neurotoxicity. Besides its beneficial effects on redox and inflammation homeostasis, this neuroprotection was accomplished by modulating the JAK2/STAT3 signaling pathway. Also, SeN's anti-apoptotic properties increased neuronal survival in both the cerebellum and SNPC. Thereby, our findings identify SeN as a highly effective and intriguing anti-neurotoxic agent, offering a new and prospective way to avoid adverse neuroinflammatory consequences.

Funding

The authors extend their appreciation to the Deanship of Research and Graduate Studies at King Khalid University for funding this work through Large Research Project under grant number RGP2/312/45.

Ethical statement

The Institutional Animal Care and Use Ethical Committee of Cairo University endorsed this study approval number (CU-III-F-65–22). All animal experiments have followed the ARRIVE guidelines and were carried out in accordance with the U.K. Animals (Scientific Procedures) Act, 1986 and associated guidelines, EU Directive 2010/63/EU for animal experiments and the National Institutes of Health guide for the care and use of Laboratory animals (NIH Publications No. 8023, revised 1978).

CRediT authorship contribution statement

Mansour A. Alghamdi: Resources, Funding acquisition. **Basma Emad Aboulhoda:** Writing – original draft, Software. **Isra H. Ali:** Formal analysis, Data curation. **Reda A. El Nasser Imam:** Investigation, Data curation, Conceptualization. **Fatma E. Hassan:** Writing – review & editing, Writing – original draft.

Declaration of Competing Interest

The authors declare no conflict of interest.

Data availability

Data will be made available on request.

Acknowledgements

The authors extend their appreciation to the Deanship of Research and Graduate Studies at King Khalid University for funding this work through Large Research Project under grant number RGP2/312/45.

Limitations of the study

Although the main target of this study was to address the neuroprotective effects of SeN against PQ-induced neurodegenerative changes, nevertheless, including a positive control group and comparisons to relevant reference group along with assessment of selenium release at tissue level still offer important information about the neuroprotective qualities and therapeutic potential of SeN. Therefore, the lack of a group receiving Se alone for comparison could be a limitation to this study to be considered in future research.

References

Abdelfattah, M.S., Badr, S.E., Lotfy, S.A., Attia, G.H., Aref, A.M., Abdel Moneim, A.E., et al., 2020. Rutin and selenium co-administration reverse 3-nitropropionic acid-induced neurochemical and molecular impairments in a mouse model of Huntington's disease. Neurotox. Res 37 (1), 77–92.

Abdraboh, M.E., Essa, Z.S., Abdelrazzak, A., El-Far, Y.M., Elsherbini, Y., El-Zayat, M.M., Ali, D.A., 2020. Radio-sensitizing effect of a cocktail of phytochemicals on HepG2 cell proliferation, motility and survival. Biomed. Pharmacother. 131, 110620 ([CrossRef] [PubMed]).

Abozaid, O.A.R., Sallam, M.W., El-Sonbaty, S., Aziza, S., Emad, B., Ahmed, E.S.A., 2022. Resveratrol-selenium nanoparticles alleviate neuroinflammation and neurotoxicity in a rat model of Alzheimer's disease by regulating Sirt1/miRNA-134/GSK3β expression. Biol. Trace Elem. Res 200 (12), 5104–5114. https://doi.org/10.1007/s12011-021-03073-7.

Al Omairi, N.E., Albrakati, A., Alsharif, K.F., Almalki, A.S., Alsanie, W., Abd Elmageed, Z. Y., et al., 2022. Selenium nanoparticles with prodi giosin rescue hippocampal damage associated with epileptic seizures induced by pentylenetetrazole in rats. Biology 11 (3), 354. https://doi.org/10.3390/biology11030354.

Alberdi, E., Sánchez-Gómez, M.V., Torre, I., Domercq, M., Pérez-Samartín, A., Pérez-Cerdá, F., Matute, C., 2006. Activation of kainate receptors sensitizes oligodendrocytes to complement attack. J. Neurosci. 26 (12), 3220–3228. Mar 22.

Albrakati, A., Alsharif, K.F., Al Omairi, N.E., Alsanie, W.F., Almalki, A.S.A., Abd Elmageed, Z.Y., et al., 2021. Neuroprotective efficiency of prodi giosins conjugated with selenium nanoparticles in rats exposed to chronic unpredictable mild stress is mediated through antioxidative, anti-inflammatory, anti-apoptotic, and neuromodulatory activities. Int J. Nanomed. 16, 8447–8464. https://doi.org/10.2147/ijn.s323436.

Al-Brakati, A., Alsharif, K.F., Alzahrani, K.J., Kabrah, S., Al-Amer, O., Oyouni, A.A., et al., 2021. Using green biosynthesized lycopene-coated selenium nanoparticles to rescue renal damage in glycerol-induced acute kidney injury in rats. Int J. Nanomed. 16, 4335.

Alhawiti, A.S., 2022. Citric acid-mediated green synthesis of selenium nanoparticles: antioxidant, antimicrobial, and anticoagulant potential applications. In: Biomass Convers Biorefinery [Internet], 0123456789. Springer Berlin Heidelberg. https://doi.org/10.1007/s13399-022-02798-2.

Ali, I.H., Elkashlan, A.M., Hammad, M.A., Hamdi, M., 2023 Dec 31. Antimicrobial and anti-SARS-CoV-2 activities of smart daclatasvir-chitosan/gelatin nanoparticles-in-PLLA nanofibrous medical textiles; in vitro, and in vivo study. In: Int J Biol Macromol, 253. Elsevier.

Amin, F., Roohbakhsh, A., Memarzia, A., Kazerani, H.R., Boskabady, M.H., 2021. Immediate and late systemic and lung effects of inhaled paraquat in rats. J. Hazard. Mater. 415, 125633.

Ashraf, H., Cossu, D., Ruberto, S., Noli, M., Jasemi, S., Simula, E.R., Sechi, L.A., 2023. Latent Potential of Multifunctional Selenium Nanoparticles in Neurological Diseases and Altered Gut Microbiota. Materials 16 (2), 699. Jan 11.

Au, A., Mojadadi, A., Shao, J.Y., Ahmad, G., Witting, P.K., 2023. Physiological benefits of novel selenium delivery via nanoparticles. Int. J. Mol. Sci. 24 (7), 6068. Mar 23.

Bai, K., Hong, B., He, J., Hong, Z., Tan, R., 2017. Preparation and antioxidant properties of selenium nanoparticles-loaded chitosan microspheres. Int J. Nanomed. 12, 4527–4539.

Banerjee, M., Chakravarty, D., Kalwani, P., Ballal, A., 2022 Nov. Voyage of selenium from environment to life: Beneficial or toxic? J. Biochem. Mol. Toxicol. 36 (11), e23195.

Blinov, A.V., Nagdalian, A.A., Siddiqui, S.A., Maglakelidze, D.G., Gvozdenko, A.A., Blinova, A.A., et al., 2022. Synthesis and characterization of selenium nanoparticles stabilized with cocamidopropyl betaine. Sci Rep [Internet]. Nature Publishing Group UK, pp. 1–16. Vol. 12, 10.1038/s41598-022-25884-x.

Brandes, M.S., Gray, N.E., 2020. NRF2 as a therapeutic target in neurodegenerative diseases, 1759091419899782–1759091419899782 ASN Neuro 12. https://doi.org/10.1177/1759091419899782.

Chen, S., Dong, Z., Cheng, M., et al., 2017a. Homocysteine exaggerates microglia activation and neuroinflammation through microglia localized STAT3 overactivation following ischemic stroke. J. Neuroinflamm. 14 (1), 187.

Chen, L., Na, R., Boldt, E., Ran, Q., 2015. NLRP3 inflammasome activation by mitochondrial reactive oxygen species plays a key role in long-term cognitive impairment induced by paraquat exposure. Neurobiol. Aging 36, 2533–2543.

Chen, J., Su, Y., Lin, F., Iqbal, M., Mehmood, K., Zhang, H., Shi, D., 2021. Effect of paraquat on cytotoxicity involved in oxidative stress and inflammatory reaction: A review of mechanisms and ecological implications. Ecotoxicol. Environ. Saf. *224*, 112711.

Chinta, S.J., Rane, A., Poksay, K.S., Bredesen, D.E., Andersen, J.K., Rao, R.V., 2008. Coupling endoplasmic reticulum stress to the cell death program in dopaminergic cells: effect of paraquat. Neuromol. Med 10 (4), 333–342. https://doi.org/10.1007/s12017-008-8047-9.

Colle, D., Farina, M., 2021. Oxidative stress in paraquat-induced damage to nervous tissues. *Toxicology*. Academic Press, pp. 69–78.

Cosentino-Gomes, D., Rocco-Machado, N., Meyer-Fernandes, J.R., 2012. Cell signaling through protein kinase c oxidation and activation. Int. J. Mol. Sci. 13, 10697–10721.

Costa, L.G., Cole, T.B., Dao, K., Chang, Y.C., Coburn, J., Garrick, J.M., 2020. Effects of air pollution on the nervous system and its possible role in neurodevelopmental and neurodegenerative disorders. Pharmacol. Ther. 2020 (210), 107523.

Cruz, D.M., Mostafavi, E., Vernet-Crua, A., O'Connell, C.P., Barabadi, H., Mobini, S., Cholula-Díaz, J.L., Guisbiers, G., García-Martín, J.M., Webster, T.J., 2023. Green nanotechnology and nanoselenium for biomedical applications. Jan 1 InNanomedicine. Woodhead Publishing, pp. 339–380. Jan 1.

Cui W. Combination of low level environmental toxicants with chemotherapeutics disturbs oligodendrocyte progenitor cell function through activation of the redox/Fyn/c-Cbl pathway (Doctoral dissertation, University of Rochester)., 2008.

Dai, Y., Liu, X., Gao, Y., 2020. Aberrant miR-219-5p is correlated with TLR4 and serves as a novel biomarker in patients with multiple organ dysfunction syndrome caused by acute paraquat poisoning. Int. J. Immunopathol. Pharmacol. *34*, 2058738420974888.

David, S., López-Vales, R., 2021. Bioactive lipid mediators in the initiation and resolution of inflammation after spinal cord injury. Neuroscience 466, 273–297. Jul 1.

Deng, Z., Jin, J., Wang, Z., Wang, Y., Gao, Q., Zhao, J., 2017. vol. Int. J. Nanomed. 12, 3617–3636.

Deng, X., Ouyang, P., Xu, W., Yang, E., Bao, Z., Wu, Y., Gong, J., Pan, J., 2023. Research progress of nano selenium in the treatment of oxidative stress injury during hepatic ischemia-reperfusion injury. Front. Pharmacol. 13, 1103483. Jan 4.

Drummond, G.R., Cai, H., Davis, M.E., Ramasamy, S., Harrison, D.G., 2000. Transcriptional and posttranscriptional regulation of endothelial nitric oxide synthase expression by hydrogen peroxide. Circ. Res 86, 347–354.

El Lateef Gharib, F.A., Zeid, I.M., Ghazi, S.M., Ahmed, E.Z., 2019. The response of cowpea (Vigna unguiculata L) plants to foliar application of sodium selenate and selenium nanoparticles (SeNPs). J. Nanomater. Mol. Nanotechnol. *8* (4).

Elfakharany, W.A., Safwat, M.M., Essawy, A.S., 2021. Possible protective and curative effects of selenium nanoparticles on testosterone-induced benign prostatic hyperplasia rat model. Folia Morphol. (Warsz.). https://doi.org/10.5603/FM.a2021.0113. Epub ahead of print. PMID: 34730228.

El-Gamal, M., Salama, M., Collins-Praino, L.E., et al., 2021. Neurotoxin-Induced Rodent Models of Parkinson's Disease: Benefits and Drawbacks. Neurotox. Res 39, 897–923.

El-Osta, H., Circu, M.L., 2016. Mitochondrial ROS and Apoptosis. In: Buhlman, L. (Ed.), Mitochondrial Mechanisms of Degeneration and Repair in Parkinson's Disease. Springer, Cham. https://doi.org/10.1007/978-3-319-42139-1_1.

Fakhrabad, M.J., Moshiri, M., Ariakia, F., Askari, V.R., Salmasi, Z., Etemad, L., 2022. Effect of cyanocobalamin (vitamin B12) on paraquat-induced brain injury in mice. Iran. J. Basic Med. Sci. *25* (6), 745.

Fan, Z., Zhang, W., Cao, Q., Zou, L., Fan, X., Qi, C., Yan, Y., Song, B., Wu, B., 2022. JAK2/STAT3 pathway regulates microglia polarization involved in hippocampal inflammatory damage due to acute paraquat exposure. Ecotoxicol. Environ. Saf. *234*, 113372 https://doi.org/10.1016/j.ecoenv.2022.113372.

Fang, J., Sheng, R., Qin, Z.H., 2021. NADPH oxidases in the central nervous system: regional and cellular localization and the possible link to brain diseases. Antioxid. Redox Signal. 35 (12), 951–973. Oct 20.

Fei, Q., McCormack, A.L., Di Monte, D.A., Ethell, D.W., 2008. Paraquat neurotoxicity is mediated by a Bak-dependent mechanism. J. Biol. Chem. 283 (6), 3357–3364. https://doi.org/10.1074/jbc.M708451200.

Firouzian, F., Pourshoja, P., Nili-Ahmadabadi, A., Ranjbar, A., 2019. Hepatoprotective effect of N-acetylcystein loaded niosomes on liver function in paraquat-induced acute poisoning. Pest. Biochem Physiol. 160, 146–153. https://doi.org/10.1016/j.pestbp.2019.08.001.

Fukushima, T., Tanaka, K., Lim, H., Moriyama, M., 2002. Mechanism of cytotoxicity of paraquat. Environ. Health Prev. Med 7 (3), 89–94 (Jul).

Gohari-Piran, M., Omidifar, N., Mohammadi, M., Nili-Ahmadabadi, A., 2022. Phlebotomy-induced iron deficiency attenuates the pulmonary toxicity of paraquat in mice. Pestic. Biochem. Physiol. *188*, 105278.

Guo, L., Xiao, J., Liu, H., Liu, H., 2020. Selenium nanoparticles alleviate hyperlipidemia and vascular injury in ApoE-deficient mice by regulating cholesterol metabolism and reducing oxidative stress. Metallomics 12, 204–217 ([CrossRef] [PubMed]).

Guzzo, C., Mat, N.F.C., Gee, K., 2010. Biol. Chem. vol. 285, 24404–24411.

Habib, M.Z., Tadros, M.G., Abd-Alkhalek, H.A., Mohamad, M.I., Eid, D.M., Hassan, F.E., Elhelaly, H., Faramawy, Y.E., Aboul-Fotouh, S., 2022. Harmine prevents 3-nitro-propionic acid-induced neurotoxicity in rats via enhancing NRF2-mediated signaling: Involvement of p21 and AMPK. Jul 15 Eur. J. Pharm. 927, 175046. https://doi.org/10.1016/j.ejphar.2022.175046. Epub 2022 May 25. PMID: 35623405.

Hamdi, M., Elkashlan, A.M., Hammad, M.A., Ali, I.H., 2023. SARS-CoV-2 Papain-like Protease Responsive ZnO / Daclatasvir-Loaded Chitosan / Gelatin Nanofibers as Smart Antimicrobial Medical Textiles: In Silico, In Vitro and Cell Studies. Pharmaceutics 15 (8), 1–25.

Hara, S., Mukai, T., Kurosaki, K., Kuriiwa, F., Yanase, T., Kano, S., et al., 2001. No parallel relationship between nitric oxide production and wet dog shakes susceptible to nitric oxide synthase inhibitors following systemic administration of paraquat in rats. Arch. Toxicol. 74, 775–782.

Hassan, F.E., Aboulhoda, B.E., Ali, I.H., Elwi, H.M., Matter, L.M., Abdallah, H.A., Khalifa, M.M., Selmy, A., Alghamdi, M.A., Morsy, S.A., Al Dreny, B.A., 2023. Evaluating the protective role of trimetazidine versus nano-trimetazidine in amelioration of bilateral renal ischemia/reperfusion induced neuro-degeneration: Implications of ERK1/2, JNK and Galectin-3/NF-κB/TNF-α/HMGB-1 signaling. Tissue Cell *85*, 102241.

Hassan, I., Ebaid, H., Al-Tamimi, J., Habila, M.A., Alhazza, I.M., Rady, A.M., 2021. Selenium nanoparticles mitigate diabetic nephropathy and pancreatopathy in rat offspring via inhibition of oxidative stress. J. King Saud. Univ. - Sci. 33 (1).

Hosseini, A., Rasaie, D., Soleymani Asl, S., Nili Ahmadabadi, A., Ranjbar, A., 2021. Evaluation of the protective effects of curcumin and nanocurcumin against lung injury induced by sub-acute exposure to paraquat in rats. Toxin Rev. 40 (4), 1233–1241. Oct 2.

Hou, L., Zhang, C., Wang, K., Liu, X., Wang, H., Che, Y., Sun, F., Zhou, X., Zhao, X., Wang, Q., 2017. Paraquat and maneb co-exposure induces noradrenergic locus coeruleus neurodegeneration through NADPH oxidase-mediated microglial activation. Toxicology 380, 1–10. https://doi.org/10.1016/j.tox.2017.02.009.

Hu, X., Li, J., Fu, M., Zhao, X., Wang, W., 2021. The JAK/STAT signaling pathway: from bench to clinic. Signal Transduct. Target Ther. 6 (1), 402. https://doi.org/10.1038/s41392-021-00791-1. PMID: 34824210; PMCID: PMC8617206.

Hu, R., Wang, X., Han, L., Lu, X., 2023. The Developments of Surface-Functionalized Selenium Nanoparticles and Their Applications in Brain Diseases Therapy. Biomimetics 8 (2), 259. Jun 15.

Huang, M., Li, Y., Wu, K., Yan, W., Tian, T., Wang, Y., Yang, H., 2019. Paraquat modulates microglia M1/M2 polarization via activation of TLR4-mediated NF-κB signaling pathway. Chem. -Biol. Interact. *310*, 108743 https://doi.org/10.1016/j.cbi.2019.108743.

Israelov, H., Ravid, O., Atrakchi, D., Rand, D., Elhaik, S., Bresler, Y., Twitto-Greenberg, R., Omesi, L., Liraz-Zaltsman, S., Gosselet, F., Schnaider Beeri, M., Cooper, I., 2020. Caspase-1 has a critical role in blood-brain barrier injury and its inhibition contributes to multifaceted repair. J. Neuroinflamm. 17, 267.

Kamaletdinova, T., Fanaei-Kahrani, Z., Wang, Z.Q., 2019. The Enigmatic Function of PARP1: From PARylation Activity to PAR Readers. Cells 8 (12), 1625. https://doi.org/10.3390/cells8121625. PMID: 31842403; PMCID: PMC6953017.

Kannaujiya, D., Vishwakarma, D., Awasthi, S., Shikha, 2023. Health Implications of Agrochemicals: Nexus of Their Impacts, Sustainable Management Approaches and Policy Gaps. InOne Health Implications of Agrochemicals and their Sustainable Alternatives. Springer Nature Singapore, Singapore, pp. 245–274.

Kao, Y.C., Ho, P.C., Tu, Y.K., Jou, I.M., Tsai, K.J., 2020. Lipids and Alzheimer's Disease. Int. J. Mol. Sci. *21* (4), 1505. https://doi.org/10.3390/ijms21041505.

Karami, M., Asri-Rezaei, S., Dormanesh, B., Nazarizadeh, A., 2018. Comparative study of radioprotective effects of selenium nanoparticles and sodium selenite in irradiation-induced nephropathy of mice model. Int J. Radiat. Biol. 94, 17–27.

Khalil, H.M.A., Azouz, R.A., Hozyen, H.F., Aljuaydi, S.H., AbuBakr, H.O., Emam, S.R., Al-Mokaddem, A.K., 2022. Selenium nanoparticles impart robust neuroprotection against deltamethrin-induced neurotoxicity in male rats by reversing behavioral alterations, oxidative damage, apoptosis, and neuronal loss. Neurotoxicology 91, 329–339. https://doi.org/10.1016/j.neuro.2022.06.006. Epub 2022 Jun 23. Erratum in: Neurotoxicology. 2023 Sep;98:98. PMID: 35753508.

Kheiripour, N., Plarak, A., Heshmati, A., Asl, S.S., Mehri, F., Ebadollahi-Natanzi, A., Ranjbar, A., Hosseini, A., 2021. Evaluation of the hepatoprotective effects of curcumin and nanocurcumin against paraquat-induced liver injury in rats:

Modulation of oxidative stress and Nrf2 pathway. J. Biochem Mol. Toxicol. 35, e22739.
Kiernan, J.A., 2000. Dyes. In: Kiernan, J.A. (Ed.), Histological and Histochemical Methods: Theory and Practice. 3rd ed. CRC Press, pp. 74–140.
Kim S., Lee S.Y., Cho H.J. Doxorubicin-Wrapped Zinc Oxide Nanoclusters for the Therapy of Colorectal Adenocarcinoma. Nanomaterials [Internet]. Multidisciplinary Digital Publishing Institute (MDPI); 2017 Nov 1 [cited 2023 Jun 9];7(354):1–13. Available from: /pmc/articles/PMC5707571/.
Kondaparthi, P., Deore, M., Naqvi, S., Flora, S.J.S., 2021. Dose-dependent hepatic toxicity and oxidative stress on exposure to nano and bulk selenium in mice. Environ. Sci. Pollut. Res 28, 53034–53044.
Kumar, M., Jaiswal, R.K., Yadava, P.K., Singh, R.P., 2020. An assessment of poly (ADP-ribose) polymerase-1 role in normal and cancer cells. Biofactors 46 (6), 894–905. https://doi.org/10.1002/biof.1688. Epub 2020 Oct 24. PMID: 33098603.
Lashgari, N.A., Roudsari, N.M., Momtaz, S., Sathyapalan, T., Abdolghaffari, A.H., Sahebkar, A., 2021. The involvement of JAK/STAT signaling pathway in the treatment of Parkinson's disease. J. Neuroimmunol. 361, 577758 https://doi.org/10.1016/j.jneuroim.2021.577758. Epub 2021 Oct 28. PMID: 34739911.
Li, L.X., Chu, J.H., Chen, X.W., Gao, P.C., Wang, Z.Y., Liu, C., et al., 2022. Selenium ameliorates mercuric chloride-induced brain damage through activating BDNF/TrKB/PI3K/AKT and inhibiting NF-κB signaling pathways. J. Inorg. Biochem 229, 111716.
Li, W.Y., Li, F.M., Zhou, Y.F., Wen, Z.M., Ma, J., Ya, K., Qian, Z.M., 2016. Aspirin down regulates hepcidin by inhibiting NF-κB and IL6/JAK2/STAT3 pathways in BV-2 microglial cells treated with lipopolysaccharide. Int. J. Mol. Sci. 17 (12), 1921.
Liu, S., Liu, K., Sun, Q., et al., 2011. Consumption of hydrogen water reduces paraquat-induced acute lung injury in rats. J. Biomed. Biotechnol. 2011, 305086.
Ma, J.-Q., Liu, C.-M., Yang, W., 2018. Protective effect of rutin against carbon tetrachloride-induced oxidative stress, inflammation and apoptosis in mouse kidney associated with the ceramide, MAPKs, p53 and calpain activities. Chem. Biol. Inter. 286, 26–33.
Mahamuni, P.P., Patil, P.M., Dhanavade, M.J., Badiger, M.V., Shadija, P.G., Lokhande, A. C., et al., 2019. Synthesis and characterization of zinc oxide nanoparticles by using polyol chemistry for their antimicrobial and antibiofilm activity. In: Biochem Biophys Reports, 17. Elsevier B.V, pp. 71–80.
McCormack, A.L., Di Monte, D.A., 2003 Apr. Effects of L-dopa and other amino acids against paraquat-induced nigrostriatal degeneration. J. Neurochem 85 (1), 82–86. https://doi.org/10.1046/j.1471-4159.2003.01621.x. PMID: 12641729.
Miller, S.J., Darji, R.Y., Walaieh, S., Lewis, J.A., Logan, R., 2023. Senolytic and senomorphic secondary metabolites as therapeutic agents in *Drosophila melanogaster* models of Parkinson's disease. Front Neurol. 14, 1271941 https://doi.org/10.3389/fneur.2023.1271941. PMID: 37840914; PMCID: PMC10568035.
Mohamed, K.M., Abdelfattah, M.S., El-khadragy, M., Al-Megrin, W.A., Fehaid, A., Kassab, R.B., Abdel Moneim, A.E., 2023. Rutin-loaded selenium nanoparticles modulated the redox status, inflammatory, and apoptotic pathways associated with pentylenetetrazole-induced epilepsy in mice. Green. Process. Synth. 12 (1), 20230010.
Naspolini, N.F., Rieg, C.E., Cenci, V.H., Cattani, D., Zamoner, A., 2021. Paraquat induces redox imbalance and disrupts glutamate and energy metabolism in the hippocampus of prepubertal rats. Neurotoxicology 85, 121–132.
Nicolas, C.S., Amici, M., Bortolotto, Z.A., Doherty, A., Csaba, Z., Fafouri, A., Dournaud, P., Gressens, P., Collingridge, G.L., Peineau, S., 2013. Jak. -Stat. vol. 2, e22925.
Nkpaa, K.W., Onyeso, G.I., Kponee, K.Z., 2019. Rutin abrogates manganese—Induced striatal and hippocampal toxicity via inhibition of iron depletion, oxidative stress, inflammation and suppressing the NF-κB signaling pathway. J. Trace Elem. Med Biol. 53, 8–15.
Nouri, A., Salehi-Vanani, N., Heidarian, E., 2021. Antioxidant, anti-inflammatory and protective potential of gallic acid against paraquat-induced liver toxicity in male rats. Avicenna J. Phytomed. 11 (6), 633.
Ortiz-Ortiz, M.A., Morán, J.M., Bravosanpedro, J.M., González-Polo, R.A., Niso-Santano, M., Anantharam, V., Kanthasamy, A.G., Soler, G., Fuentes, J.M., 2009. Curcumin enhances paraquat-induced apoptosis of N27 mesencephalic cells via the generation of reactive oxygen species. Neurotoxicology 30 (6), 1008–1018. https://doi.org/10.1016/j.neuro.2009.07.016. Epub 2009 Aug 4. PMID: 19660496; PMCID: PMC2789857.
Ossowska, K., Wardas, J., Smiałowska, M., Kuter, K., Lenda, T., Wierońska, J.M., Zieba, B., Nowak, P., Dabrowska, J., Bortel, A., Kwieciński, A., Wolfarth, S., 2005. A slowly developing dysfunction of dopaminergic nigrostriatal neurons induced by long-term paraquat administration in rats: an animal model of preclinical stages of Parkinson's disease? Eur. J. Neurosci. 22 (6), 1294–1304. https://doi.org/10.1111/j.1460-9568.2005.04301.x. PMID: 16190885.
Oztürk, Z., Gurpinar, T., Vural, K., Boyacıoglu, S., Korkmaz, M., Var, A., 2015. Effects of selenium on endothelial dysfunction and metabolic profile in low dose streptozotocin induced diabetic rats fed a high fat diet. Biotech. Histochem 90 (7), 506–515. https://doi.org/10.3109/10520295.2015.1042050. Epub 2015 May 15. PMID: 25978137.
Patro, N., Patro, I., Tandon, P.N., 2022. Oligodendrocyte: Structure, Function and Pathology. The Biology of Glial Cells: Recent Advances. Springer Singapore, Singapore, pp. 45–73.
Rand, D., Cooper, I., 2021. Caspase-1: an important player and possible target for repair of the blood-brain barrier underlying neurodegeneration. Neural Regen. Res 16 (12), 2390–2392. https://doi.org/10.4103/1673-5374.313031. PMID: 33907012; PMCID: PMC8374582.
Reinke, S., Linge, M., Diebner, H.H., Luksch, H., Glage, S., Gocht, A., Robertson, A.A.B., Cooper, M.A., Hofmann, S.R., Naumann, R., Sarov, M., Behrendt, R., Roers, A., Pessler, F., Roesler, J., Rösen-Wolff, A., Winkler, S., 2020. Non-canonical caspase-1 signaling drives RIP2-dependent and TNF-αmediated inflammation in vivo. Cell Rep. 30, 2501–2511 e5.
Ren, B., Liu, M., Ni, J., Tian, J., 2018. Role of Selenoprotein F in Protein Folding and Secretion: Potential Involvement in Human Disease. Nutrients 10 (11), 1619. https://doi.org/10.3390/nu10111619. PMID: 30400132; PMCID: PMC6266307.
Rusek, M., Smith, J., El-Khatib, K., Aikins, K., Czuczwar, S.J., Pluta, R., 2023. The Role of the JAK/STAT Signaling Pathway in the Pathogenesis of Alzheimer's Disease: New Potential Treatment Target. Int J. Mol. Sci. 24 (1), 864. https://doi.org/10.3390/ijms24010864. PMID: 36614305; PMCID: PMC9821184.
Salaramoli, S., Amiri, H., Joshaghani, H.R., Hosseini, M., Hashemy, S.I., 2023. Bio-synthesized selenium nanoparticles ameliorate Brain oxidative stress in Parkinson disease rat models. Metab. Brain Dis. May 3:1-0.
See, W.Z.C., Naidu, R., Tang, K.S., 2022. Cellular and molecular events leading to paraquat-induced apoptosis: mechanistic insights into Parkinson's disease pathophysiology. Mol. Neurobiol. 59, 3353–3369. https://doi.org/10.1007/s12035-022-02799-2.
Shen, Y., Huang, H., Wang, Y., Yang, R., Ke, X., 2022. Antioxidant effects of Se-glutathione peroxidase in alcoholic liver disease. J. Trace Elem. Med. Biol., 127048
Silva, J., Alves, C., Soledade, F., Martins, A., Pinteus, S., Gaspar, H., Alfonso, A., Pedrosa, R., 2023. Marine-Derived Components: Can They Be a Potential Therapeutic Approach to Parkinson's Disease? Mar. Drugs 21 (8), 451.
Sivagurunathan, N., Gnanasekaran, P., Calivarathan, L., 2023. Mitochondrial Toxicant-Induced Neuronal Apoptosis in Parkinson's Disease: What We Know so Far. Degener. Neurol. Neuromuscul. Dis. 1–3.
Smeyne, R.J., Breckenridge, C.B., Beck, M., Jiao, Y., Butt, M.T., Wolf, J.C., Zadory, D., Minnema, D.J., Sturgess, N.C., Travis, K.Z., Cook, A.R., Smith, L.L., Botham, P.A., 2016. Assessment of the Effects of MPTP and Paraquat on Dopaminergic Neurons and Microglia in the Substantia Nigra Pars Compacta of C57BL/6 Mice. PLoS One 11 (10), e0164094.
Somayajulu-Nițu, M., Sandhu, J.K., Cohen, J., Sikorska, M., Sridhar, T.S., Matei, A., Borowy-Borowski, H., Pandey, S., 2009. Paraquat induces oxidative stress, neuronal loss in substantia nigra region and parkinsonism in adult rats: neuroprotection and amelioration of symptoms by water-soluble formulation of coenzyme Q10. BMC Neurosci. 10, 88. https://doi.org/10.1186/1471-2202-10-88. PMID: 19635141; PMCID: PMC2724477.
Srivastav, S., Fatima, M., Mondal, A.C., 2018. Bacopa monnieri alleviates paraquat induced toxicity in Drosophila by inhibiting jnk mediated apoptosis through improved mitochondrial function and redox stabilization. Neurochem Int 121, 98–107. https://doi.org/10.1016/j.neuint.2018.10.001.
Su, Y., Huang, X., Huang, Z., et al., 2020. STAT3 localizes in mitochondria-associated ER membranes instead of in mitochondria. Front. Cell Dev. Biol. 8, 274.
Tahavvori, A., Gargari, M.K., Yazdani, Y., Mamalo, A.S., Beilankouhi, E.A., Valilo, M., 2023. Involvement of antioxidant enzymes in Parkinson's disease. Pathol. -Res. Pract., 154757
Thabet, N.M., Moustafa, E.M., 2018. Protective effect of rutin against brain injury induced by acrylamide or gamma radiation: Role of PI3K/AKT/GSK-3β/NRF-2 signalling pathway. Arch. Physiol. Biochem 124 (2), 185–193. https://doi.org/10.1080/13813455.2017.1374978Search.
Tong, T., Duan, W., Xu, Y., Hong, H., Xu, J., Fu, G., Wang, X., Yang, L., Deng, P., Zhang, J., He, H., 2022. Paraquat exposure induces Parkinsonism by altering lipid profile and evoking neuroinflammation in the midbrain. Environ. Int. 169, 107512.
Trempe, J.F., Gehring, K., 2023. Structural mechanisms of mitochondrial quality control mediated by PINK1 and parkin. J. Mol. Biol. (12), 168090
Wang, K., Liu, Y., Shi, Y., Yan, M., Rengarajan, T., Feng, X., 2021. Amomum tsaoko fruit extract exerts anticonvulsant effects through suppression of oxidative stress and neuroinflammation in a pentylenetetrazol kindling model of epilepsy in mice. Saudi J. Biol. Sci. 28 (8), 4247–4254.
Wang, Q., Ren, N., Cai, Z., Lin, Q., Wang, Z., Zhang, Q., Wu, S., Li, H., 2017. Paraquat and MPTP induce neurodegeneration and alteration in the expression profile of microRNAs: the role of transcription factor Nrf2. NPJ Park. Dis. 3, 31. https://doi.org/10.1038/s41531-017-0033-1. PMID: 29071302; PMCID: PMC5651826.
Wartenberg, M., Schallenberg, M., Hescheler, J., Sauer, H., 2003. Reactive oxygen species-mediated regulation of eNOS and iNOS expression in multicellular prostate tumor spheroids. Int J. Cancer 104, 274–282.
Wu, B., Song, B., Yang, H., Huang, B., Chi, B., Guo, Y., Liu, H., 2013. Central nervous system damage due to acute paraquat poisoning: an experimental study with rat model. Neurotoxicology 35, 62–70.
Yang, L., Cui, Y., Liang, H., Li, Z., Wang, N., Wang, Y., Zheng, G., 2022. Multifunctional selenium nanoparticles with different surface modifications ameliorate neuroinflammation through the gut Microbiota-NLRP3 Inflammasome-Brain axis in APP/PS1 mice. ACS Appl. Mater. Interfaces 14 (27), 30557–30570.
Yuan, X., Fu, Z., Ji, P., Guo, L., Al-Ghamdy, A.O., Alkandiri, A., et al., 2020. Selenium nanoparticles pre-treatment reverse behavioral, oxidative damage, neuronal loss and neurochemical alterations in pentylenetetrazole-induced epileptic seizures in mice. Int J. Nanomed. 15, 6339–6353.
Yue, D., Zeng, C., Okyere, S.K., Chen, Z., Hu, Y., 2021. Glycine nano-sele nium prevents brain oxidative stress and neurobehavioral abnormalities caused by MPTP in rats. J. Trace Elem. Med Biol. 64, 126680 https://doi.org/10.1016/j.jtemb.2020.126680.
Zeng, X.S., Geng, W.S., Jia, J.J., 2018. Neurotoxin-induced animal models of parkinson disease: pathogenic mechanism and assessment. ASN Neuro 10, 1759091418777438.
Zhang, Y., Yuan, D., Li, Y., Yang, F., Hou, L., Yu, Y., Sun, C., Duan, G., Meng, C., Yan, H., Li, D., Gao, Y., Sun, T., Zhu, C., 2021. Paraquat promotes acute lung injury in rats by

regulating alveolar macrophage polarization through glycolysis. Ecotoxicol. Environ. Saf. *223*, 112571 https://doi.org/10.1016/j.ecoenv.2021.112571.

Zhen, J., Lu, H., Wang, X.Q., Vaziri, N.D., Zhou, X.J., 2008. Upregulation of endothelial and inducible nitric oxide synthase expression by reactive oxygen species. Am. J. Hypertens. 21, 28–34.

Zhong, Y., Yin, B., Ye, Y., Dekhel, O.Y.A.T., Xiong, X., Jian, Z., Gu, L., 2021. The bidirectional role of the JAK2/STAT3 signaling pathway and related mechanisms in cerebral ischemia-reperfusion injury. Exp. Neurol. 341, 113690 https://doi.org/10.1016/j.expneurol.2021.113690. Epub 2021 Mar 31. PMID: 33798563.